Extreme Summer Convection in South America

ULRIKE ROMATSCHKE

University of Washington, Seattle, Washington, and University of Vienna, Vienna, Austria

ROBERT A. HOUZE JR.

University of Washington, Seattle, Washington

(Manuscript received 6 October 2009, in final form 4 February 2010)

ABSTRACT

Tropical Rainfall Measuring Mission (TRMM) Precipitation Radar (PR) and National Centers for Environmental Prediction–National Center for Atmospheric Research (NCEP–NCAR) reanalysis data are used to indicate mechanisms responsible for extreme summer convection over South America. The three-dimensional reflectivity field is analyzed to define three types of extreme echo, *deep convective cores, wide convective cores*, and *broad stratiform regions*. The location and timing of these echoes are sensitive to midlatitude synoptic disturbances crossing the Andes. At the leading edges of these disturbances the nocturnal South American low-level jet (SALLJ) transports moisture along the eastern edge of the Andes from the tropical to the subtropical part of the continent. Where the SALLJ rises over lower but steep mountains on the east side of the southern central Andes, deep and wide convective cores are triggered in the evening. When the SALLJ withdraws to the north as the disturbance passes, nocturnal triggering occurs in the northeastern foothills of the central Andes. Extreme convection over the Amazon basin takes the form of broad stratiform regions that evolve from systems with wide convective cores moving into the center of the region from both the southwest and northeast. The systems from the northeast form at the northeast coast and are likely squall lines. Along the coast of the Brazilian Highlands, diurnal/topographic forcing leads to daytime maxima of deep convective cores followed a few hours later by wide convective cores. Wide convective cores and broad stratiform regions form in the South Atlantic convergence zone (SACZ) with a diurnal cycle related to continental heating.

1. Introduction

South America features some of the most extreme convective cloud systems on the planet. Zipser et al. (2006) have pointed out that some of the deepest convective systems on Earth occur in Argentina near the Andes. Garstang et al. (1994) showed that some of the largest squall lines in the world occur over the Amazon region. These extreme vertical and horizontal structures occur in a region where massive topography and complex land surface characteristics affect the convection. The 3- to almost 7-km-high north–south-oriented Andes are effectively a wall separating the low-level suppressed flow of the southeast Pacific from the unstable low-level flow dominating weather over the tropical and subtropical portions of the continent (Fig. 1). The Brazilian Highlands in the eastern part of the continent, though not as vertically extensive, cover a broad area and further constrain the airflow and heating patterns. In between and around these elevated areas, the lowlands are characterized by the two main river basins—the La Plata basin (PLB) in the subtropics and the massive Amazon basin (AMZ) in the tropics (Fig. 1a), with the tropical rain forests of the latter providing a large amount of moisture.

Knowledge of the details of convection throughout the tropics and subtropics has been revolutionized by analysis of data from the Tropical Rainfall Measuring Mission (TRMM) satellite's Precipitation Radar [PR; see Kummerow et al. (1998) for a description of the TRMM instruments]. Zipser et al. (2006) have shown the overall distribution of extreme convection, and Houze et al. (2007) and Romatschke et al. (2010) have analyzed the

Corresponding author address: Ulrike Romatschke, Atmospheric Sciences, P.O. Box 351640, University of Washington, Seattle, WA 98195-1640.
E-mail: ulli@atmos.washington.edu

DOI: 10.1175/2010JCLI3465.1

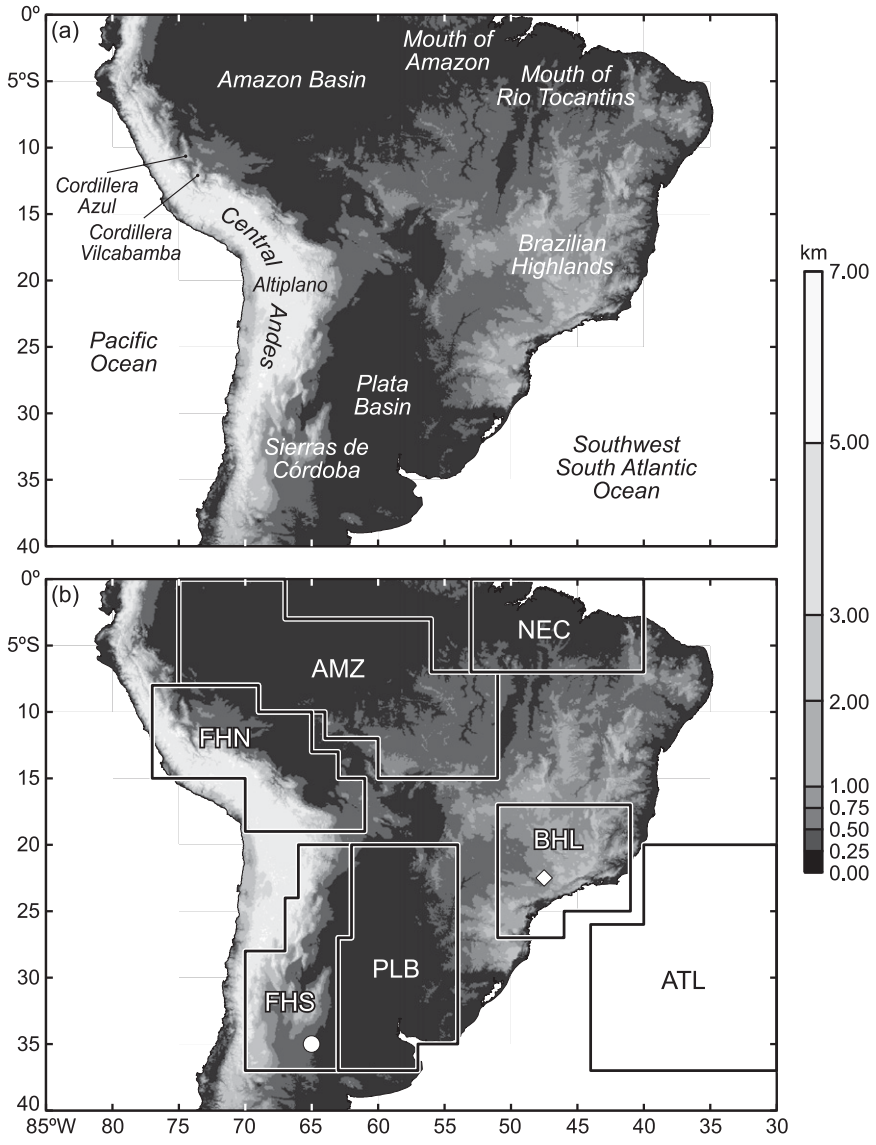

FIG. 1. Region of this study: (a) relevant topographical features, (b) regions studied in detail: PLB, FHS, FHN, AMZ, NEC, BHL, and ATL. The white circle and diamond mark the locations of the soundings shown in Figs. 12 and 16, respectively.

extreme convection over South Asia using PR data to define specific types of extreme convective structure. They related the occurrence of extreme convection to the synoptic-scale flow, the complex topography, and the diurnal cycle of the region. In this study, we will apply similar techniques to determine the characteristics of extreme convection over South America. The methodology, described in detail in Romatschke et al. (2010), used the PR's uniformly excellent vertical resolution and its ability to separate convective and stratiform precipitation (Awaka et al. 1997) to identify echo elements indicative of convective cloud systems containing extremely intense convection and extremely robust stratiform precipitation.

Figure 2 shows the summer precipitation and extreme convection climatology compiled from TRMM data for South America (see section 2 for a detailed description of the datasets used). The red frame in Fig. 2a encloses the area of this study, which includes all of the areas of significant summer precipitation and extremely intense convection (as identified by Zipser et al. 2006; Fig. 2b) over the continent. Comparison of the two figure panels shows that in the subtropical zone of the continent the extremely deep and intense convection is located in a climatological minimum of precipitation. On the other hand, the studies of Garstang et al. (1994) and Machado et al. (1998) indicate that robust mesoscale convective

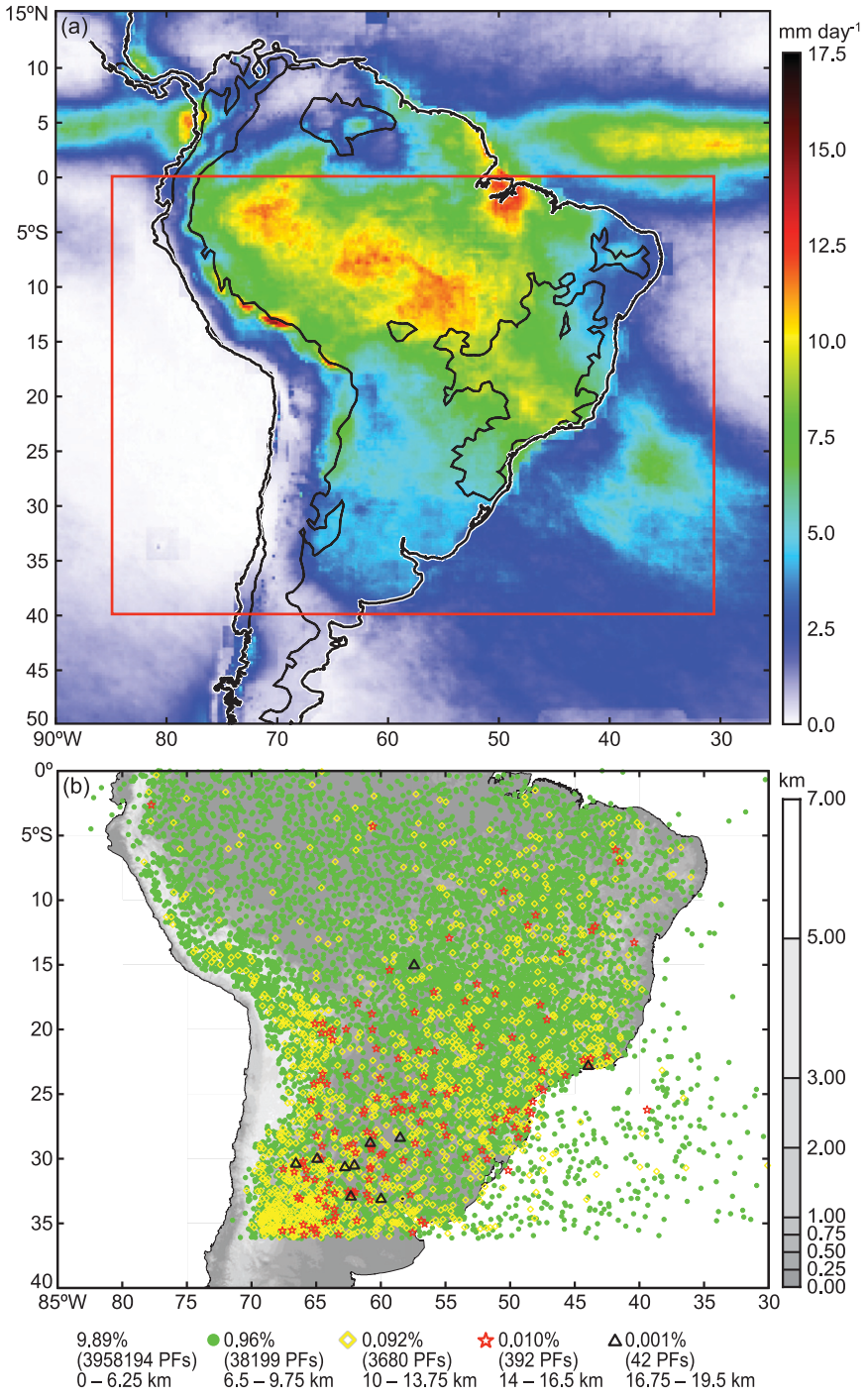

FIG. 2. (a) DJF precipitation climatology from TRMM product 3B43. The studied region (red square) is shown. (b) Location of intense convective precipitation features (PFs; Liu et al. 2008) as identified by the maximum height of the 40-dBZ TRMM PR radar echo (km). Different colors show the frequency of the PFs in different intensity bins. The summer months of 9 yr (1998–2006) are used. Modified from Zipser et al. (2006).

systems (MCSs) occur in the tropical Amazonian area of maximum rain. This comparison illustrates that the problem of understanding extreme convective processes in the atmosphere is distinct from explaining patterns and amounts of precipitation. The rainfall pattern and occurrence of severe weather events overlap but do not coincide. Understanding the convective mechanisms will likely help to understand the precipitation mechanisms leading to the precipitation climatology. However, our focus in this paper is not on estimating or explaining precipitation amounts, but rather on seeking insight into the mechanisms leading to the extreme forms of summer convection in South America. Understanding the well-defined extreme forms of convection, characterized by both their vertical extent [associated with severe weather (Zipser et al. 2006) but little precipitation] and horizontal extent [associated with severe weather (Garstang et al. 1994) and heavy precipitation], is a first step toward a comprehensive understanding of all of the convective processes contributing to severe weather and rainfall in South America.

Previous studies of convection over South America have emphasized the importance of certain large-scale flow patterns (Vera et al. 2006). In the northern tropical region of the continent, large-scale easterlies prevail as a westward extension of the South Atlantic subtropical high. The massive squall-line systems described by Garstang et al. (1994) occur in that environment. Nogués-Paegle and Mo (1997), Garreaud and Wallace (1998), Liebmann et al. (1999), and Garreaud (2000) have noted the importance of the passage of baroclinic troughs across the Andes and the associated low-level flow pattern during the passages. Ahead of the troughs, the South American low-level jet (SALLJ) extends southward along the eastern foothills of the Andes toward the portion of the La Plata basin noted for severe convection (Fig. 2b; see also Saulo et al. 2000). These strong synoptic forcings must be considered to fully understand the extreme convection over South America. Studies of the diurnal cycle show daytime maxima of convection and precipitation over most of the continental areas (Garreaud and Wallace 1997; Kikuchi and Wang 2008). Important exceptions are nocturnal maxima over the La Plata basin and along the eastern Andes foothills (Kikuchi and Wang 2008), emphasizing the important role of the terrain in the development (Lenters and Cook 1995) and timing of convection.

This paper therefore examines the frequency of occurrence of extreme radar echoes and determines how the occurrence of these echoes relates to synoptic forcing, complex topography, and the diurnal heating cycle over and near South America. To gain insight into the mechanisms leading to extreme convection in different regions, we use data from the TRMM PR to document the spatial and temporal variability of extreme convection and large-scale reanalysis data to document the synoptic situations in which the convection occurs. We follow the methodology of Houze et al. (2007) and Romatschke et al. (2010) in using the three-dimensional structure of TRMM PR echoes to determine metrics of convective intensity. Then, we analyze the frequency of occurrence of these extreme radar echo metrics for the summer season in relationship to varying synoptic conditions, mountains, and the solar cycle.

2. Data and methods of analysis

a. NCEP–NCAR reanalysis data for synoptic-scale background

National Centers for Environmental Prediction–National Center for Atmospheric Research (NCEP–NCAR) reanalysis data (Kalnay et al. 1996) were used to study the synoptic conditions associated with enhanced convection. Long-term monthly mean data (1968–96) show the seasonal mean fields. Composites of daily and 4-times-daily data were generated to explore the synoptic anomalies and the diurnal cycle. Soundings were extracted from the composites. Because of the lack of observations in the Southern Hemisphere and its coarse resolution, the dataset, and especially the diurnal variations, should be used with caution. However, the reanalysis is known to capture the general characteristics of the atmosphere even in the vicinity of the steep and narrow Andes Mountains (Marengo et al. 2004), and the results from analyzing the data make sense physically.

b. TRMM data for identifying extreme convective types

The austral summer months [December–February (DJF)] for 10 yr (from December 1998 to February 2008) of various types of TRMM data (Kummerow et al. 2000, 1998) in our region of interest (0°–40°S, 30°–85°W, Fig. 1) are used. All data are version 6. Data from before and after the satellite boost from 350 to 403 km, which took place from 7 to 24 August 2001, are processed the same way. Specifically, we use the following:

- Level 2 PR products 2A23 [rain characteristics; see Awaka et al. (1997)] and 2A25 [rainfall rate and profile; see Kozu et al. (2000) and Iguchi et al. (2000)] provide the rain-type classification (i.e., convective–stratiform) and the three-dimensional (3D) attenuation-corrected reflectivity field, respectively. These products are the datasets we use to identify categories of extreme convection. To facilitate the analysis, we first reprocess the data products by remapping the reflectivity

and rain-type classification onto a latitude–longitude grid with 0.05° × 0.05° (~5 km × 5 km) horizontal and 0.25-km vertical resolution using the technique described in Houze et al. (2007) and Romatschke et al. (2010).
- Level 3 product 3A25 [spaceborne radar rainfall; see Meneghini et al. (2001)] provides monthly rainfall, which is used to calculate a seasonal precipitation climatology, and the number of radar gates on a 0.5° × 0.5° grid. The latter is used to normalize the reflectivity data according to the strongly latitude-dependent sampling frequency (Romatschke et al. 2010).
- Level 3 products 3B42 (TRMM and other GPCP calibration rainfall) and 3B43 [TRMM and other sources rainfall (Huffman et al. 2007)] provide 3-hourly and monthly rainfall estimates on a 0.25° × 0.25° grid, respectively. They are used to calculate 3-hourly and seasonal precipitation climatologies.

c. *Definition of deep convective cores, wide convective cores, and broad stratiform regions*

To identify convective echoes that develop extreme characteristics of intensity, height, or horizontal extent, we extract three types of radar echo structures from the TRMM PR 2A25 reflectivity. Details about the exact identification and classification process are described in Romatschke et al. (2010). Briefly, we first separate the data into convective and stratiform echoes, as defined by the 2A23 product. Within the convective echo category, we identify the most intense echoes by extracting all 3D echo volumes that consist entirely of reflectivity values of 40 dBZ or greater. Any such echo is called a ''convective core.'' Within the convective core dataset, we identify the following two subcategories:

- *Deep convective cores* are convective cores whose maximum heights are ≥10 km above mean sea level (MSL). They are most likely young and vigorous convective cells with strong updrafts of the type that are often associated with severe weather.
- *Wide convective cores* are convective cores that extend over an area of ≥1000 km^2 when projected onto a horizontal plane. They are often parts of large MCSs in an early, strongly convective stage of their life cycle (Houze 2004).

Within the stratiform echo category we identify one subcategory, as follows:

- *Broad stratiform regions* are said to exist whenever a contiguous stratiform 3D echo volume extends over an area of ≥50 000 km^2 when projected on a horizontal plane. They are often parts of extremely large MCSs in a late, stratiform stage of their life cycle (Houze 2004).

3. Climatological setting

During the summer months, upper-level wind patterns over the region of study (Fig. 1, red frame in Fig. 2a) are characterized by a 200-mb anticyclone centered just east of the central Andes (the Bolivian high) and the western edge of the South Atlantic low to the east (Fig. 3a). At 500 mb (Fig. 3b), the easterly and westerly winds to the north and south respectively are pronounced, illustrating that the South American continent is characterized by a tropical climate with easterlies in its northern latitudes and a midlatitude/subtropical climate with strong midlevel westerlies in its southern reaches. A transport of air from south to north with low moisture content occurs along the eastern side of the Bolivian high. Two regions of higher moisture are found over the Altiplano and the Amazon basin. The influence of the continent and the Andes become pronounced at the 700-mb level (Fig. 3c). The easterly winds to the north turn northwesterly along the Andes, probably influenced by the channeling effect of the Andes, although Lenters and Cook (1995) attribute this circular wind pattern primarily to the effect of the continental low rather than to the effect of the Andes. Over the Brazilian Highlands and the eastern part of the South Atlantic the northwesterly winds merge with the midlatitude westerlies to form the South Atlantic convergence zone (SACZ), which is associated with strong precipitation (Fig. 2b).

The summertime mean surface wind pattern contains several features that are key to understanding the occurrence of extreme convection in South America (Fig. 3d). Along the west coast of South America, winds have an anticyclonic curvature and a strong south–north component associated with the subtropical high over the South Pacific. However, these winds do not cross the Andes and do not have any direct effect on the convection over the continent east of the Andes. On the east coast, the surface winds have a generally easterly component, which makes them important in understanding convective occurrence over the continent. In the southern (subtropical) latitudes, the surface winds penetrate landward, bringing moist oceanic air into the La Plata basin and the southern region of the central Andes. In the northern (tropical) latitudes, the surface winds penetrate inland for some distance, but weaken abruptly so that the interior Amazon region is characterized broadly by light surface winds and low-level convergence. On the western side of the Amazon basin, along the eastern foothills of the Andes, northerly component winds parallel the mountains and advect moisture from the Amazon to the southern part of the continent. This feature is the climatological manifestation of the SALLJ. The strength of these northerlies, which is connected to the passage of synoptic-scale

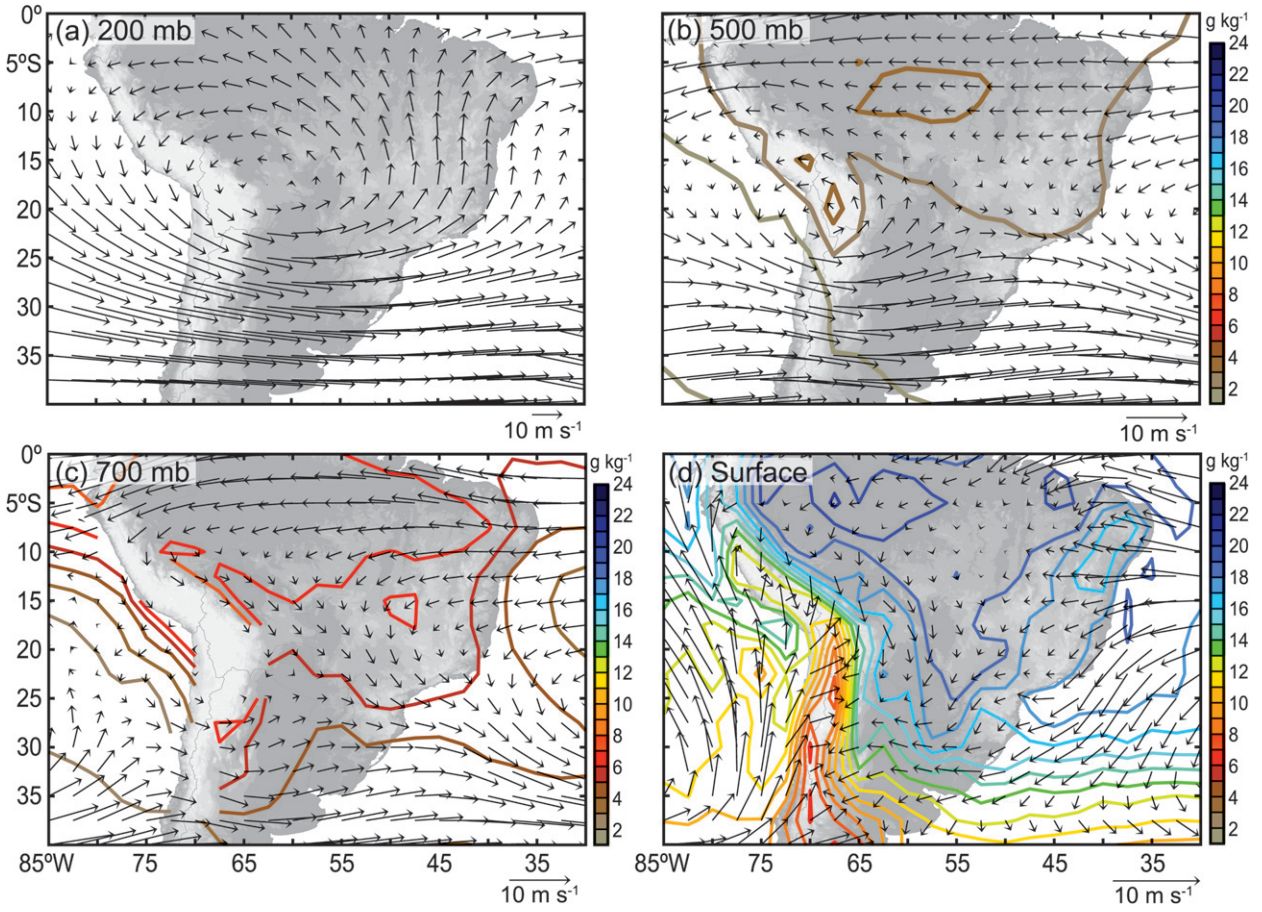

FIG. 3. DJF NCEP–NCAR climatology of specific humidity (g kg^{-1}) and winds (m s^{-1}) at (a) 200 mb (the specific humidity is not available at this level), (b) 500 mb, (c) 700 mb, and (d) surface level. Data points intersecting the terrain are excluded.

disturbances, has a profound influence on the location of extreme convection over the whole continent as will be presented in section 5.

In the seasonal mean, heating over the Andes forces the low-level wind upslope, which converges over the mountains (Fig. 3d). Figure 4 shows that the just-described surface wind pattern is not observed during all times of the day. Although the heating of the terrain during the afternoon and evening hours leads to upslope flow and convergence over the mountains (Figs. 4c,d) in the seasonal mean (Fig. 3d), these conditions are actually reversed at night and in the morning (Figs. 4a,b). Radiative cooling leads to divergence at high elevations and downslope flow. Also, the SALLJ, which is weakened during the daytime by the convergence over the mountains and the resulting upslope flow, and probably by turbulent mixing, is strongest during the night (Fig. 4a). This climatology suggests that the diurnal cycle plays an important role in the mechanisms leading to convection and precipitation. We examine the diurnal cycle in detail in section 6.

4. Overall frequency of occurrence of extreme radar echo structures

Figure 5 shows the spatial distribution of the three categories of radar echo structures defined in section 2c. Plotted is the probability of finding an echo structure in each 0.5° × 0.5° grid box. The probability is normalized to the sampling frequency of the TRMM satellite as described in Romatschke et al. (2010).

a. Deep convective cores

Deep convective cores (Fig. 5a) are found most frequently in the subtropical part of the continent, consistent with Zipser et al. (2006; see also Fig. 2b). These echo structures occur with maximum frequency in the western La Plata basin and the southeastern foothills of the central Andes, and extend into the northeast to the southern part of the Brazilian Highlands (BHL; Fig. 1a) and to the South American east coast. This region of intense convection lies near the climatological intersection of the SALLJ and the upper-level strong

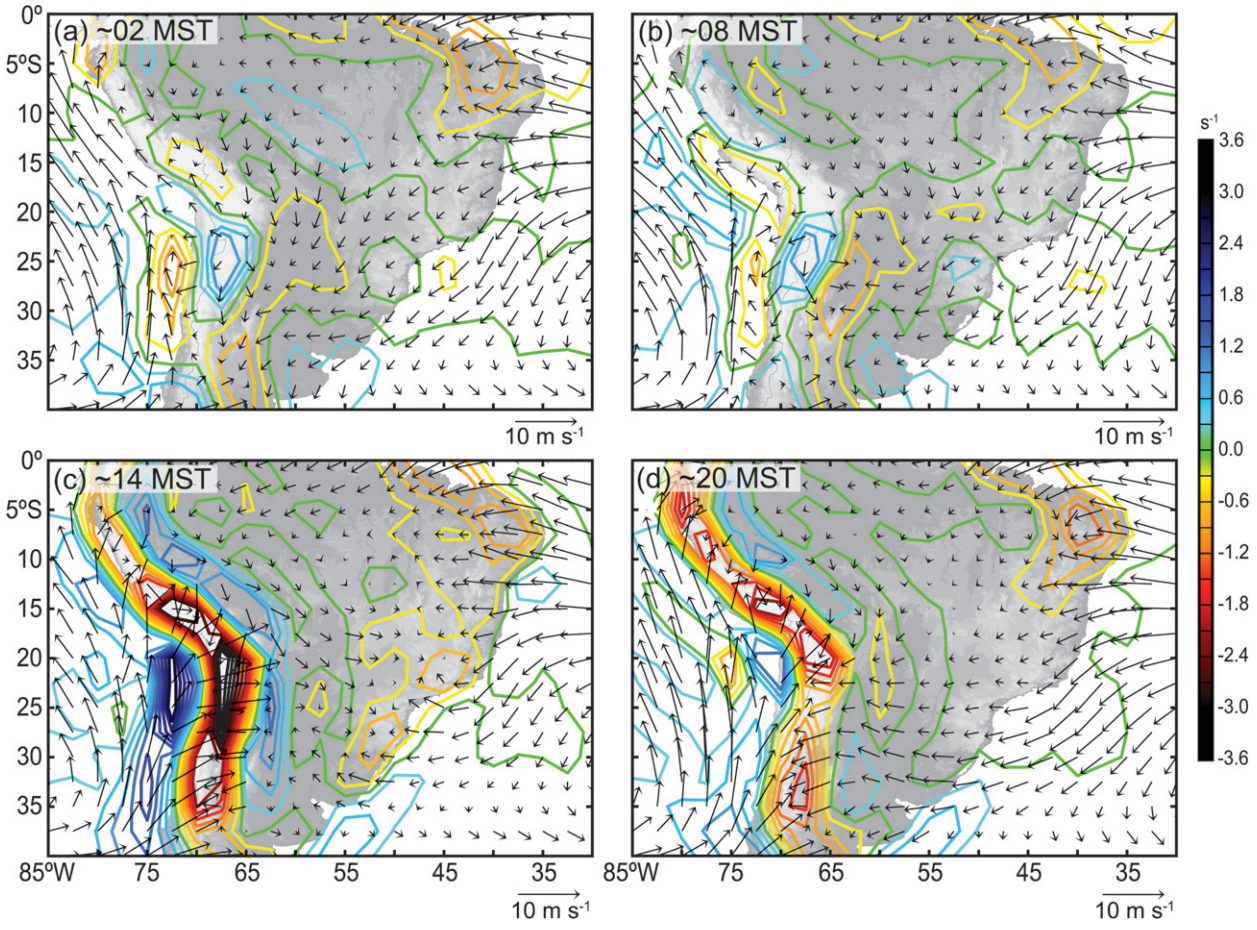

FIG. 4. DJF NCEP–NCAR surface winds (m s^{-1}) and divergence (s^{-1}) at (a) 0600 UTC (~0200 MST), (b) 1200 UTC (~0800 MST), (c) 1800 UTC (~1400 MST), and (d) 0000 UTC (~2000 MST).

westerlies seen in the wind climatology at 200 mb in Fig. 3a.

Despite the dryness of the area (Fig. 3d), deep convective cores also occur over the Altiplano, although their total vertical extent is less, owing to the high elevation of the underlying terrain. A similar occurrence of deep convective cores was observed over the Tibetan Plateau during the South Asian monsoon by Houze et al. (2007) and Romatschke et al. (2010).

b. *Wide convective cores*

Wide convective cores occur with maximum frequency in the La Plata basin in a region that overlaps with the maximum occurrence of deep convective cores (Fig. 5b). An additional subtropical maximum frequency of wide convective cores is observed over the Atlantic Ocean in association with the SACZ. Deep convective cores are extremely rare in this oceanic region (Fig. 5a), just as they are rare in the oceanic regions surrounding the South Asian subcontinent (Romatschke et al. 2010). A minimum in the frequency of wide convective cores is observed just offshore from the Brazilian Highlands, probably as a result of downslope flow suppressing convection in the lee of the highlands (Fig. 3c). In tropical regions, secondary maxima in the frequency of wide convective cores are observed along the northeastern foothills of the central Andes and over the broad expanse of the Amazon basin.

c. *Broad stratiform regions*

The locations of the maxima in broad stratiform regions (Fig. 5c) are very similar to those in wide convective cores, although their intensity is very different. They occur over 1) the northeastern foothills of the central Andes and the Amazon basin, 2) the SACZ and the Brazilian Highlands, and 3) the La Plata basin. The centroid of the latter maximum is shifted to the east of the center of the maximum frequency of wide convective cores (cf. Figs. 5b,c). This farther shift eastward suggests that the broad stratiform regions reflect eastward-moving

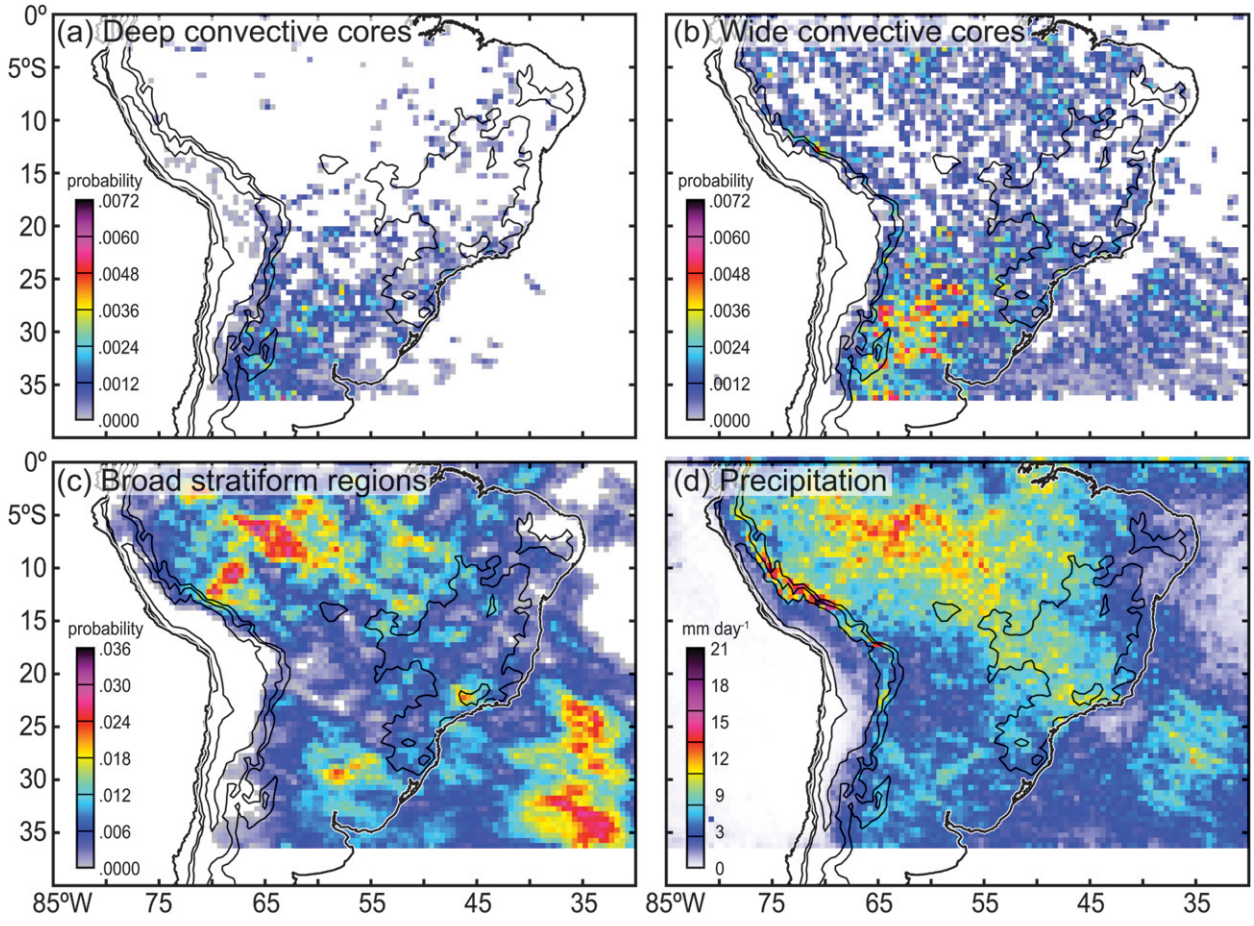

FIG. 5. Geographical distribution of the probability of finding (a) a deep convective core, (b) a wide convective core, and (c) a broad stratiform region. Note the different color scales. (d) DJF precipitation climatology from the TRMM PR product 3A25. Topographic contours of 0.3, 1.5, and 3 km are shown (black).

MCSs in later stages of development. It is especially apparent that, unlike deep and wide convective cores, which do not correlate with rainfall, the frequency pattern of broad stratiform regions coincides closely with the pattern of rain accumulation over the entire region of interest (Fig. 5d), suggesting that the broad stratiform regions are parts of the large MCSs that are the major rain producers over the continent (Ashley et al. 2003; Fritsch et al. 1986; Garstang et al. 1994).

d. Selection of subregions

Based on the patterns of occurrence of deep convective cores, wide convective cores, and broad stratiform regions, as well as the precipitation climatology (Figs. 5a–d), we select the seven regions shown in Fig. 1b to investigate the synoptic, topographic, and diurnal processes that affect the occurrence of different types of extreme convective systems. These regions enclose maximum occurrence of one or more types of radar echo structures and/or precipitation. They are the PLB, the southern and northern foothills of the central Andes (FHS and FHN, respectively), the AMZ, the northeastern coast (NEC), the BHL, and the Atlantic Ocean region just off the coast of Brazil (ATL). The NEC was chosen because a precipitation maximum in the 3B43 combined precipitation product occurs along this coast (Fig. 2a). This maximum may be overestimated by this product, because it does not show nearly so strongly in the 3A25 product (Fig. 5d), which is based solely on the PR. In any case, none of the categories of extreme radar echo structures tend to occur in the NEC, so this maximum must be due to generally less intense convection. This region is also of interest because of the tendency of squall lines to form in this zone. Often the precipitation maxima over the northern half of the continent, that is, in the AMZ and BHL regions, are considered to be an extension of the SACZ. However, the precipitation mechanisms over land are substantially different than those over the ocean, and we consider them separately from the oceanic SACZ in the ATL region, as

TABLE 1. Numbers of echo structures in each category and region and corresponding numbers of days in composites. Bold numbers represent the categories and regions further investigated in this study.

	Number of radar echo structures							
	Total	PLB	FHS	FHN	AMZ	NEC	BHL	ATL
Deep convective	1237	**328**	**518**	35	18	12	**114**	2
Wide convective	2898	**707**	**502**	**126**	**245**	**112**	**173**	**330**
Broad stratiform	902	**123**	17	**46**	**128**	34	**43**	**290**
				Number of days in composites				
Deep convective		180	227				83	
Wide convective		313	254	98	182	96	130	178
Broad stratiform		95		44	119		40	200

has been done previously, for example, by Carvalho et al. (2004). The numbers of echo structures in each region and category are shown in Table 1. The echo structures in the categories and regions whose numbers are printed in bold are considered to occur frequently enough to be further investigated.

5. Synoptic forcing

To investigate the influence of the synoptic conditions on the occurrence of the different types of radar echo structures defined in section 2c, composites of NCEP–NCAR reanalysis fields for the regions and echo structure types printed in bold in Table 1 were constructed. Because some days have several occurrences of the same echo structure type, the number of days in the composites is smaller than the number of echo structures (Table 1). Four-times-daily surface wind composites were produced to study the influence of different wind regimes and their diurnal variation. Daily 500-mb geopotential height anomalies (i.e., composite minus seasonal mean) and surface pressure anomalies show the position of mid- and low-level disturbances.

Our examination of the data in this study suggests that the presence or absence of the SALLJ, in connection with a midlatitude low passing through, has an important influence on the occurrence of convection in South America, especially in the FHS and PLB regions (section 5a). Figure 6 therefore shows composites of NCEP–NCAR surface reanalysis data for the time of day when the SALLJ is strongest, that is, ~0200 Mean Solar Time (MST;[1] Marengo et al. 2004). Although some previous studies have tended to focus on the 850-mb winds to characterize the SALLJ, we chose to analyze surface wind data (from the sigma 0.995 reanalysis level) because the 850-mb level intersects with the terrain at the location of the Andes.

According to Table 1, our analysis encompasses 21 separate combinations of echo structure type and region, 15 of which are further investigated because of their higher frequency. Figures 6 and 7 show the surface wind, geopotential height, and surface pressure anomaly composites for four of these combinations. The four panels in Fig. 6 and the corresponding four lines in Fig. 7 represent situations when systems with wide convective cores, which have the largest samples (Table 1), were occurring in the FHS, PLB, FHN, and ATL regions. We do not show all 15 such patterns because these examples represent four canonical patterns, and each of the 15 combinations of echo structure type and region occurred in one of these canonical pattern types or variations thereof, which are described in the following subsections.

a. Trough, SALLJ, and extreme convection over the subtropical continent (FHS and PLB)

Figures 6a,b and 7a–d show ~0200 MST and daily composites respectively, for days when wide convective cores were observed in the FHS and PLB regions. The composite wind patterns for the deep convective cores in the FHS and deep convective cores and broad stratiform regions in the PLB are very similar to those for the wide convective cores and are therefore not shown. The following discussion of the composites for the wide convective cores is therefore considered representative for all three categories of radar echo structures in the FHS and PLB regions.

In the FHS composite (Fig. 6a), the SALLJ is pronounced along the eastern slopes of the central Andes foothills and is stronger than that in the climatological mean (cf. Figs. 4a and 6a). The corresponding 500-mb geopotential height anomaly (Fig. 7a) shows anomalously low geopotential heights centered over the southern Andes and extending over the Altiplano to the north. At the surface (Fig. 7b), anomalously low pressure is

[1] The local time used in this study is Mean Solar Time, which is solely a function of longitude [MST (min) = UTC (min) + longitude × 4 (min)], where longitude east is positive and longitude west is negative; UTC times are converted to ~MST by subtracting 4 h.

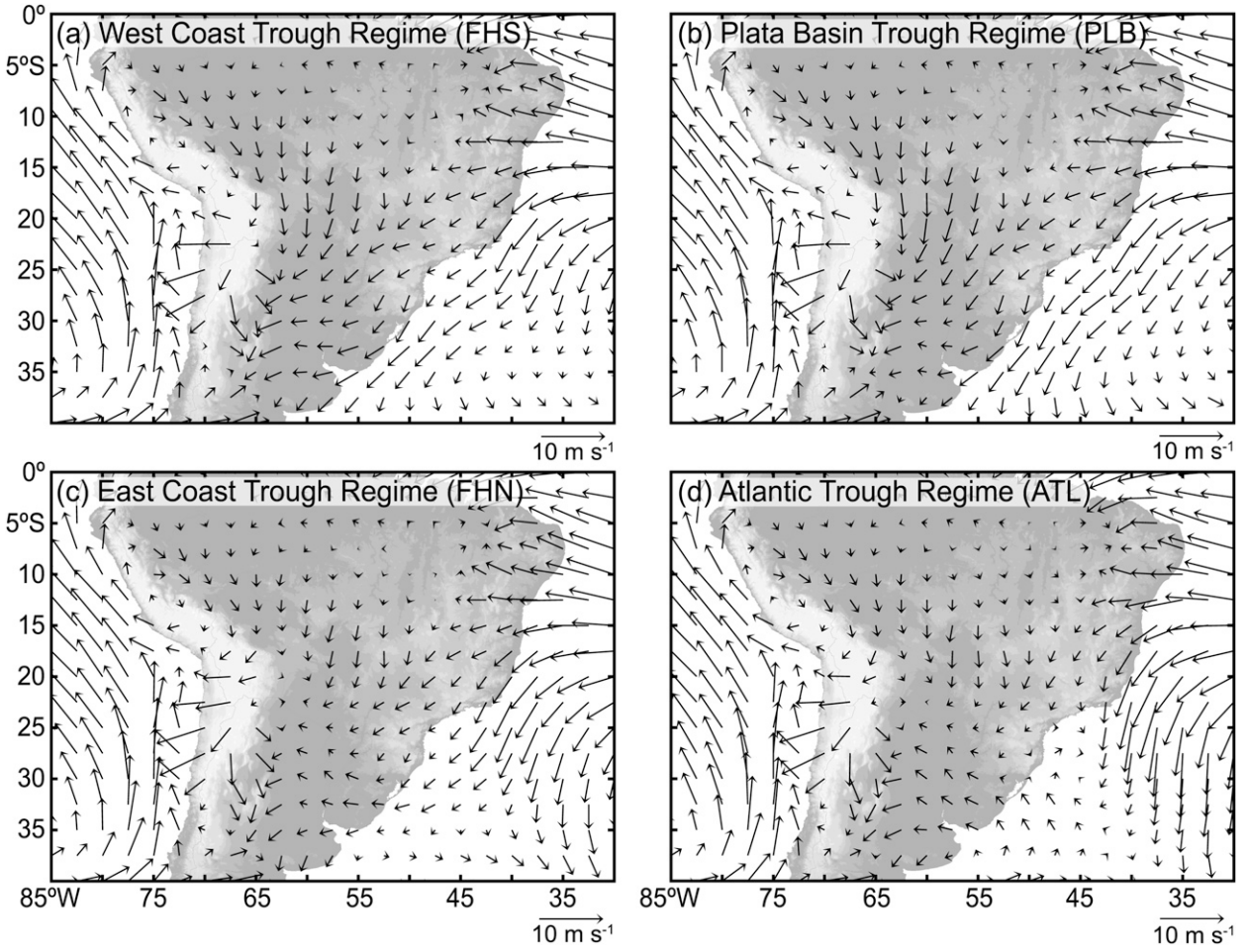

FIG. 6. Composite of NCEP–NCAR reanalysis 0600 UTC (~0200 MST) surface winds for days when wide convective cores occurred within the (a) FHS, (b) PLB, (c) FHN, and (d) ATL regions.

found over the La Plata basin and along the eastern Andes foothills just ahead of the midlevel trough. Because of the position of the anomalous geopotential low at 500 mb in Fig. 7a, we call this synoptic setting the ''west coast trough regime.'' Reading Fig. 7 down the page, one gains the impression that the anomaly patterns show the stages of a trough passage across South America, even though these composites were drawn from different cases. In Figs. 7c,d, the anomalous midlevel and surface lows are shifted eastward, centered over the southern and eastern La Plata basin, respectively. We call this synoptic setting the ''La Plata basin trough regime.''

The west coast and La Plata basin trough regimes, representing the first two stages of a trough passage, are consistent with findings by Garreaud and Wallace (1998), which show that the west coast and La Plata basin trough regimes resemble the early stages (i.e., their days −2, −1.5, and −1, where day 0 represents the most intense convection located at the northeastern edge of the La Plata basin and the southwestern edge of the Brazilian Highlands) of a summertime incursion of colder midlatitude air into tropical regions in association with a midlatitude trough passing through [see also the conceptual model in Fig. 10 of Garreaud (2000)]. They show an enhancement of the convective index (CI) over the La Plata basin and stronger northerly low-level winds (i.e., the SALLJ) along the eastern foothills of the central Andes on day −1.5. Liebmann et al. (1999) draw a similar picture, linking the trough passage to a Rossby wave originating in the Southern Hemisphere westerlies, which turns equatorward as it crosses the Andes (Liebmann et al. 2004).

The SALLJ, which is strengthened ahead of troughs in synoptic settings like the west coast and the La Plata basin trough regimes (Figs. 6a,b and 7a–d), is known to advect moisture from the tropics to the subtropical plains and to increase the convergence over the La Plata basin (Salio et al. 2007). These mechanisms, together with

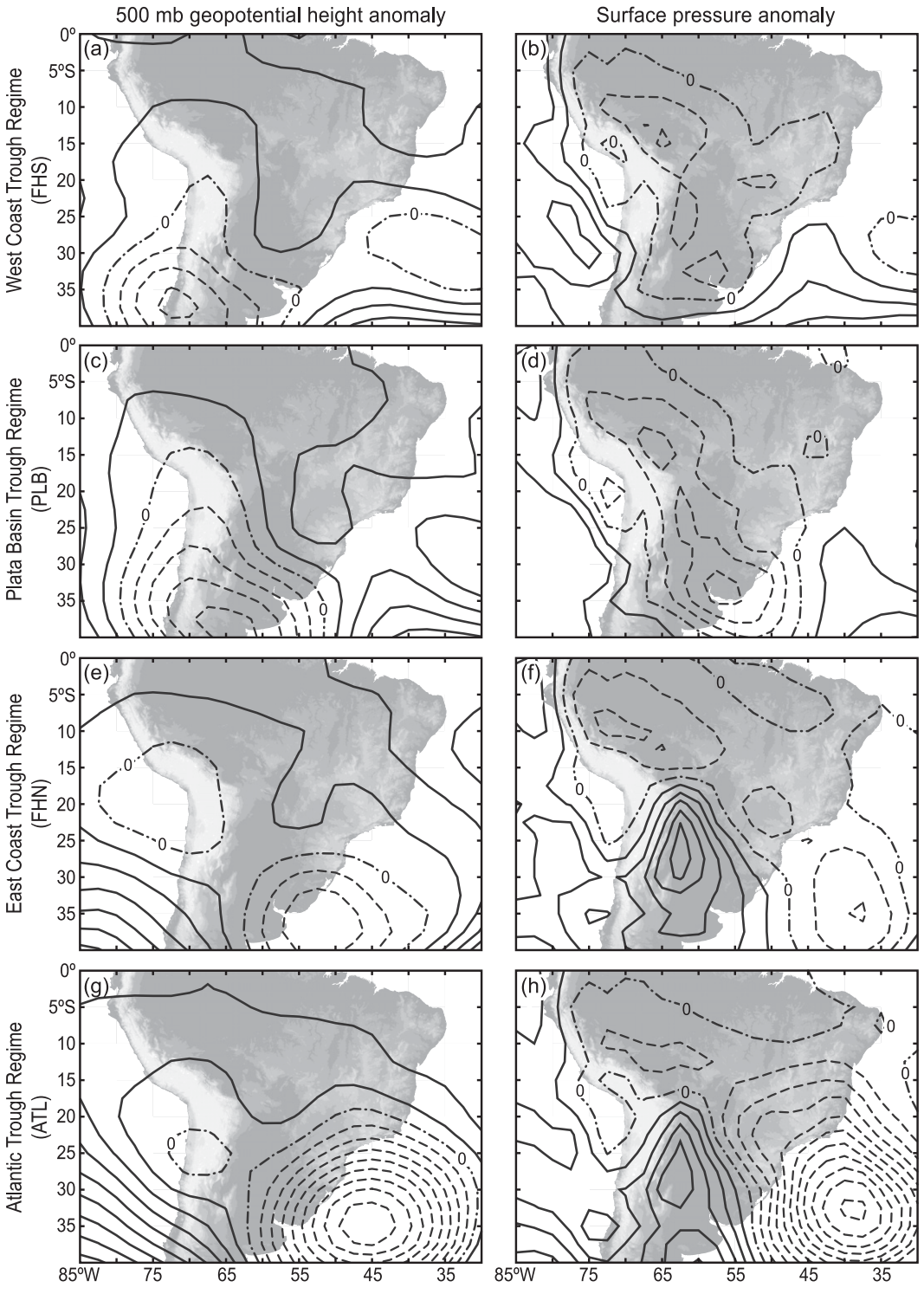

FIG. 7. Composite of NCEP–NCAR reanalysis geopotential height anomalies at (left) 500 mb and (right) surface pressure anomalies for days when wide convective cores occurred within the (a),(b) FHS, (c),(d) PLB, (e),(f) FHN, and (g),(h) ATL regions. Contour intervals are (left) 4 m and (right) 4 mb, with negative contours dashed and the zero contour dash–dotted.

baroclinic zones associated with the trough passages, are linked to the occurrence of our extreme convection categories. Others have noted the association of the SALLJ with enhanced development of MCSs (Salio et al. 2007), mesoscale convective complexes (MCCs) (Velasco and Fritsch 1987), ''large, long-lived convective cloud systems (LLCSs)'' (Nieto Ferreira et al. 2003), positive rainfall anomalies (Liebmann et al. 2004), negative outgoing longwave radiation (OLR) anomalies (Marengo et al. 2004), and convection, represented by infrared (IR) brightness temperature thresholds, moving from west to east (Salio et al. 2007) over the southern part of the continent. The extreme convection categories identified in this study (Fig. 5) statistically quantify the timing, location, size, and intensity of extreme convection phenomena in this region so that they can be related more precisely to the SALLJ and other synoptic, topographic, and diurnal features.

The shear in wind speed and direction between the SALLJ and the upper-level westerlies is evident in the climatology (Fig. 3) and is enhanced when the SALLJ is strengthened. Westerly flow passing over high terrain overrides low-level unstable moist flow until lifting of the low-level flow over the topography of the Sierras de Córdoba (Fig. 1a) releases the instability. This sheared environment favors extreme convection (Rosenfeld et al. 2006), severe storms and tornadoes (Altinger de Schwarzkopf and Rosso 1982), and the development of eastward-propagating mesoscale squall-line systems (Anabor et al. 2008), and will be further discussed in section 6a(2). These conditions are somewhat analogous to severe storm environments over the United States (Carlson et al. 1983) and South Asia (Houze et al. 2007; Medina et al. 2010; Romatschke et al. 2010).

b. *Trough moves eastward and extreme convection occurs in northern latitudes (FHN, AMZ, NEC, and BHL)*

A very different synoptic setting is found when extreme convection occurs in the FHN region (Figs. 6c and 7e,f). The SALLJ exists only along the northern foothills of the central Andes and is completely absent in the subtropics (Fig. 6c). The negative geopotential height anomaly at the 500-mb level is located over the east coast, that is, farther east than in the La Plata basin trough regime (cf. Figs. 7c,e). At the surface, anomalous low pressure extends from the western part of the South Atlantic northwestward to the northern foothills of the central Andes (Fig. 7f). The low pressure anomalies over the La Plata basin found in the west coast and La Plata basin trough regimes (Figs. 7b,d) are replaced by strong anomalous high pressure whose anticyclonic wind anomalies counteract the SALLJ. This pattern shuts down the moisture flow from the Amazon basin to the La Plata basin, and mass and moisture pile up instead along the northern foothills of the central Andes. Convection in the FHN is probably triggered as the SALLJ, which is now restricted to the tropics, is lifted over the foothills. We call this synoptic setting the ''east coast trough regime.'' It is consistent with the synoptic conditions at a later stage of a trough passage (Garreaud 2000; Garreaud and Wallace 1998; Liebmann et al. 1999). Enhancement of extreme convection in the northern latitudes in this type of synoptic setting agrees with Nieto Ferreira et al. (2003), who observed more LLCSs in the northern latitudes in connection with weak SALLJs.

The composite wind patterns for situations in which wide convective cores and broad stratiform regions are present in the AMZ and NEC regions have synoptic-scale characteristics similar to those of the east coast trough regime (Figs. 6c and 7e,f) and are therefore not shown. However, in the AMZ and NEC composites the SALLJ extends a little farther south, and the surface pressure and 500-mb height anomalies are somewhat weaker. These differences might be due to the fact that some days with conditions similar to the mean climatology or even the west coast or the La Plata basin trough regimes described in the previous subsection are part of the composites. This suggests that the synoptic situation and especially the SALLJ play a less important role in the occurrence of extreme convection over the AMZ and NEC than in the FHN. This inference is further strengthened by the fact that there is little difference in the surface wind fields over the AMZ and NEC regions between the west coast, the La Plata basin, and the east coast trough regimes (cf. Figs. 6a,b and 6c).

Over the BHL, the composites for the broad stratiform regions are also similar to those for the east coast trough regime (Figs. 6d and 7e,f). However, the anomalous lows at 500 mb and the surface are stronger and centered over the southern part of the Brazilian Highlands, that is, farther north than in the east coast trough regime. This difference suggests that the exact location of the extreme convection is sensitive to the position of the synoptic-scale low. Local cyclogenesis, as observed by Gan and Rao (1991), might also play a role in this region. Consistent with our east coast trough regime, Garreaud and Wallace (1998) found positive CI anomalies over the southwestern Amazon basin and the Brazilian Highlands on their days 0 and 1 of a trough passage. The composites for the wide convective cores over the BHL are also comparable to those for the east coast trough regime, but with weaker anomalies and the SALLJ extending farther south. The same is true for the BHL deep convective core composites, which, in addition, do not show the high surface pressure anomaly over the La Plata

basin. These results suggest that the synoptic regime and the location of the midlevel trough, while important for the formation of systems containing broad stratiform regions, have limited influence on the formation of wide and especially of deep convective cores in the BHL.

As a final comment, we note that analyses of the extensive datasets collected during the TRMM Large-Scale Biosphere–Atmosphere (TRMM-LBA) field campaign, which was conducted in the southern Amazon basin in January and February 1999 (Silva Dias et al. 2002), also show the influence of the synoptic conditions on the location of convection. Remote sensing data (Carvalho et al. 2002; Gan et al. 2004; Jones and Carvalho 2002; Laurent et al. 2002; Petersen et al. 2002) as well as various in situ measurements (Cifelli et al. 2002; Halverson et al. 2002; Pereira and Rutledge 2006; Rickenbach et al. 2002) underline the importance of different wind regimes on the formation of convection in different regions. However, these studies classify the synoptic patterns into westerly and easterly wind regimes resulting from the prevailing local zonal wind or wind anomaly direction at low levels over the TRMM-LBA domain (~11°S, ~62°W) rather than according to larger synoptic patterns. Because of the fact that the TRMM-LBA domain is in the northern part of the SALLJ region, this definition does not differentiate between the existence or absence or different directions of the southern part of the SALLJ, which are likely sensitive to the exact location of the midlatitude disturbance. Therefore, the westerly and easterly wind regime categories of TRMM-LBA are not directly comparable to our west coast/La Plata basin and east coast trough regimes.

c. *Offshore convection excited when trough moves beyond the coast (ATL)*

Figure 6d shows the wind composite for the wide convective cores in the ATL region. Because of the absence of the SALLJ it resembles the east coast trough regime. However, there is a converging wind pattern over the eastern part of the South Atlantic in a northwest-to-southeast direction that is not evident in the east coast trough regime composite (Fig. 6c). The geopotential height (Fig. 7g) and pressure anomalies (Fig. 7h) show a strong low in mid- and low levels at the same location as the wind convergence (i.e., the oceanic part of the SACZ). We call this synoptic setting the ''Atlantic trough regime.'' Again, the composite fields for the broad stratiform regions are very similar to the composites for the wide convective cores and therefore are not shown.

The Atlantic trough regime compares to the latest stage of a trough passage [e.g., days 1 and 1.5 in Garreaud and Wallace (1998)]. Liebmann et al. (2004) link the strengthening of the SACZ not only to a midlatitude wave train but also to the Madden–Julian oscillation (MJO; Madden and Julian 1994).

6. Topographic and diurnal effects

This section explores how the diurnal heating and the effect of the topography combine with the synoptic conditions described in the previous section to favor or disfavor extreme convection. Even when looking only at the surface winds and their divergence (Fig. 4) it is evident that the diurnal heating, especially over mountainous areas, must have a profound effect on the occurrence of convection. This impression is confirmed by plotting the diurnal cycle of the TRMM 3B42 precipitation data (Fig. 8), which shows precipitation maxima in different regions at different times of the day. To study the effects of the diurnal heating on the occurrence of extreme convection and precipitation, Figs. 9–11 show the occurrence of deep and wide convective cores and broad stratiform regions, respectively, in 6-h intervals centered on the synoptic times of ~2000, 0200, 0800, and 1400 MST. For reference, the subregions defined in section 4d are outlined in red in these figures. Because the diurnal behavior of extreme convection varies regionally, the following subsections examine the diurnal behavior of each type of extreme convection in each of the subregions in detail.

a. *Diurnal triggering of deep convection over the Sierras de Córdoba and FHS, followed by the development and progression of mesoscale systems across the PLB*

Extreme convection occurs in the FHS and PLB regions in the synoptic settings of the west coast and La Plata basin trough regimes (section 5a). The timing and form of this convection is tightly controlled by the topography and solar cycle.

1) REGIONAL VARIABILITY OF THE DIURNAL CYCLE OF EXTREME CONVECTION

In the early afternoon deep and wide convective cores are evenly distributed over both the PLB and the FHS regions, probably as a result of daytime solar heating (Figs. 9c and 10c). A strong maximum in occurrence of deep and wide convective cores is observed in the 6 h centered on ~2000 MST over the Sierras de Córdoba (Figs. 1, 9d, and 10d). This maximum extends to the north over the Andes foothills and east over the entire La Plata basin within the next several hours (Figs. 9a and 10a,b). The maximum in deep convective cores is gone in the morning, although a few deep convective cores still appear over the central La Plata basin (Fig. 9b). The maximum in wide convective cores is more persistent and

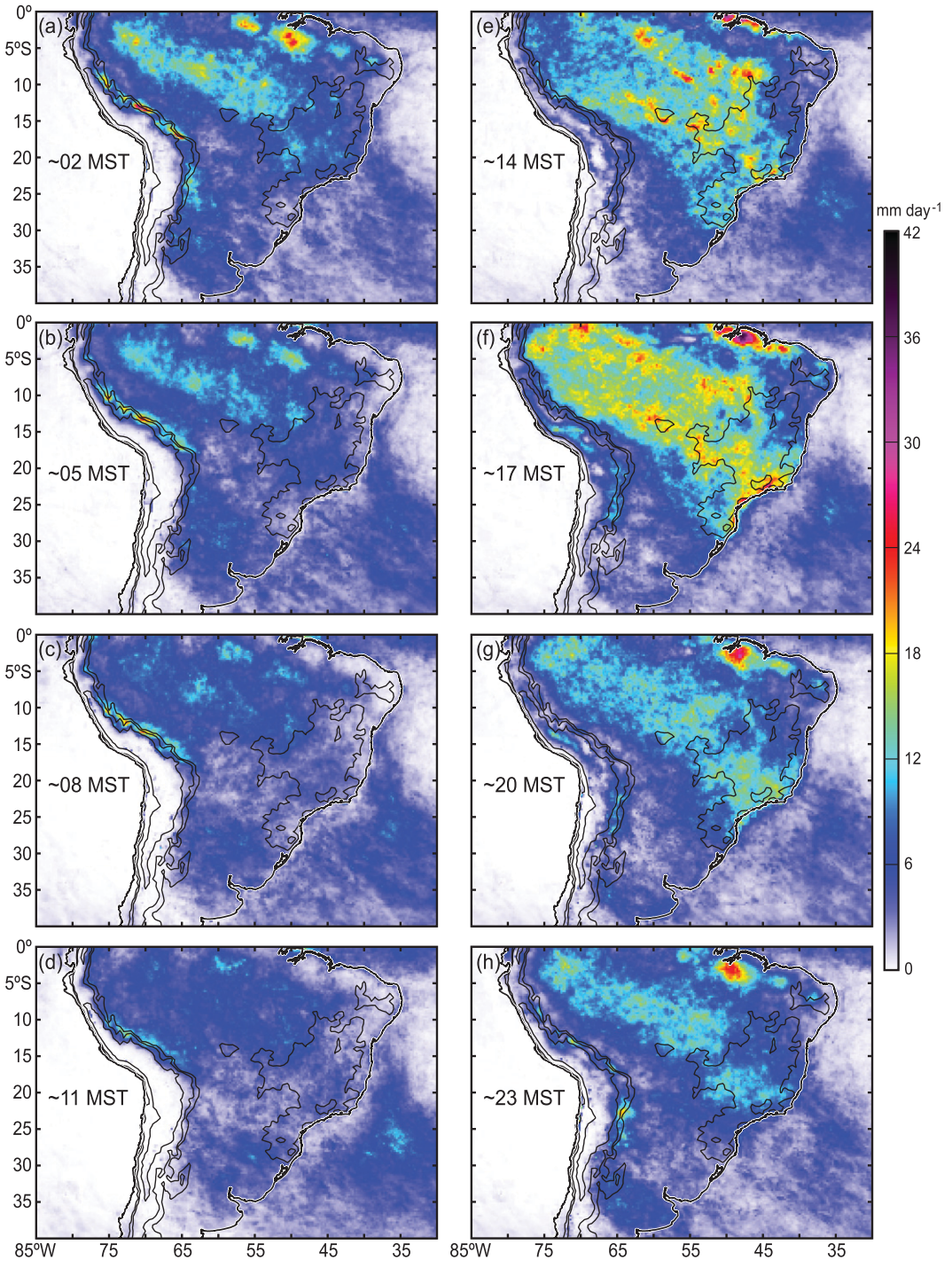

FIG. 8. DJF precipitation climatology from TRMM product 3B42 for (a) 0600 UTC (~0200 MST), (b) 0900 UTC (~0500 MST), (c) 1200 UTC (~0800 MST), (d) 1500 UTC (~1100 MST), (e) 1800 UTC (~1400 MST), (f) 2100 UTC (~1700 MST), (g) 0000 UTC (~2000 MST), and (h) 0300 UTC (~2300 MST). Topographic contours as in Fig. 5.

extends farther east during the morning hours (Fig. 10b). Broad stratiform regions are rare in the FHS but show a strong maximum in the morning to early afternoon hours in the southeastern PLB (Figs. 11b,c). This maximum coincides with the maximum of wide convective cores at this time of day in this region.

The patterns just described suggest a phenomenological sequence in which the deep convective cores occur

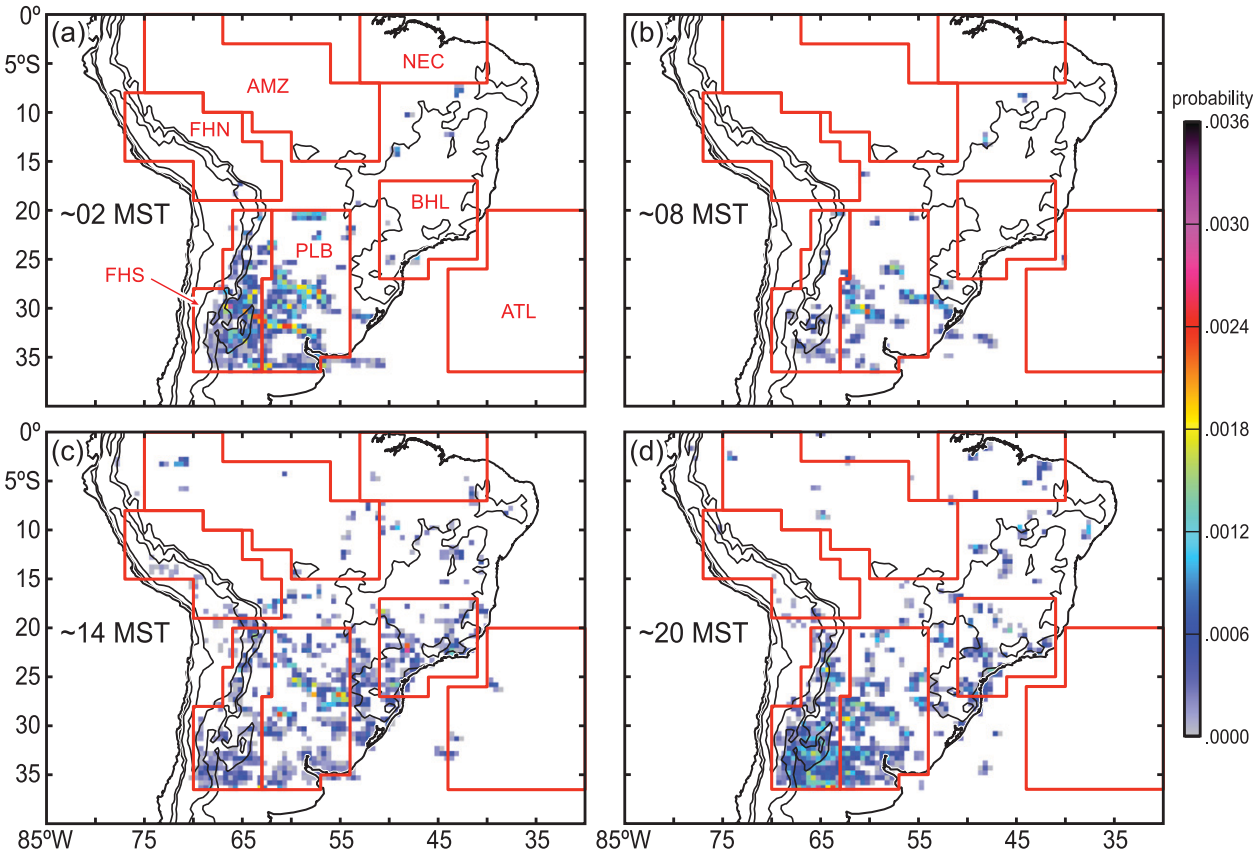

FIG. 9. Geographical distribution of the probability of finding a deep convective core between 3 h prior to and 3 h after (a) 0600 UTC (~0200 MST), (b) 1200 UTC (~0800 MST), (c) 1800 UTC (~1400 MST), and (d) 0000 UTC (~2000 MST). Topographic contours as in Fig. 5.

in the vicinity of the Sierras de Córdoba as part of the early triggering phase of convective systems, some of which develop into eastward-moving MCSs that manifest wide convective cores during their mature phase over the La Plata basin. The eastward movement of MCSs would be expected in light of the strong westerlies at 500 mb in this region (Fig. 3b). A similar evolution is observed in the precipitation climatology. A precipitation maximum found in the evening over the Sierras de Córdoba (Figs. 8g,h) extends to the north and east during the several next hours (Figs. 8a,b) and extends over the eastern La Plata basin in the morning (Figs. 8c,d) before it dissipates in the afternoon (Figs. 8e,f).

Analysis of infrared satellite data by Anabor et al. (2008) is consistent with the different categories of extreme convection observed in our study representing different stages in the life cycle of MCSs and shows via case study analysis how the convective evolution relates to the synoptic-scale forcing. The storms that evolve into the MCSs studied by Anabor et al. (2008) were frequently triggered near the Sierras de Córdoba around 2100 Local Time (LT) in connection with a surface low pressure system located east of the Andes. We also find the maximum occurrence of the deep convective cores in the late evening over the Sierras de Córdoba and the subsequent maximum occurrence of wide convective cores and broad stratiform regions over the La Plata basin to coincide with a synoptic-scale low east of the Andes (section 5a and Fig. 7d). Anabor et al. (2008) also found northerly surface winds advecting moist air along the eastern foothills of the Andes, as we have seen in the composite wind analysis (Fig. 6b). They observe "individual systems moving to the east or southeast, yet the region of convective development as a whole shifts to the north or northwest . . . ," which agrees with our observations. They found the maximum extent of the MCSs to occur around 0800 LT to the east of the location of the triggering, consistent with the maximum occurrence of broad stratiform regions seen in our statistical results (Fig. 11b). At this stage they find that the surface low had become less intense and moved eastward. The MCSs dissipated to the northeast, already outside of our PLB region, as the surface low in the La Plata basin is replaced by a high, corresponding to our east coast trough regime

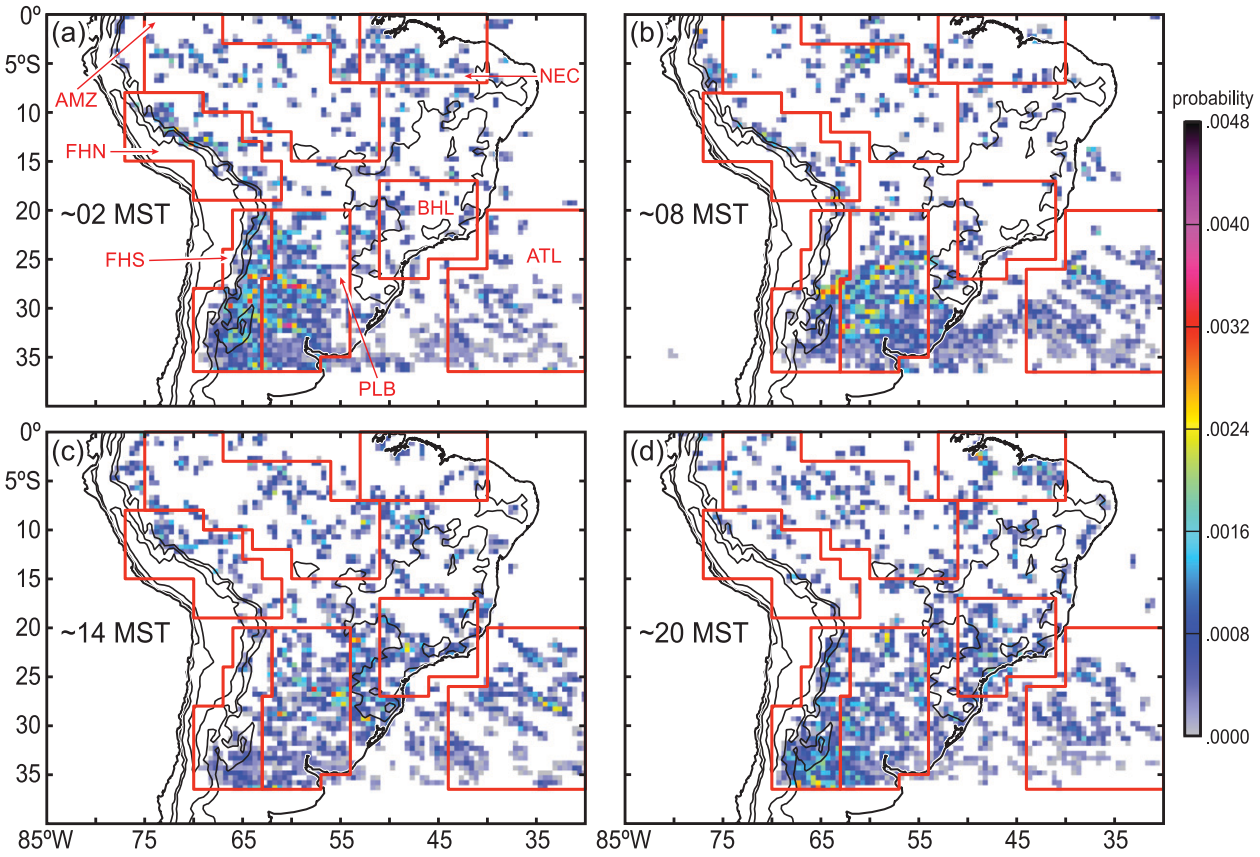

FIG. 10. As in Fig. 9, but for wide convective cores.

(section 5b and Fig. 7c). The synoptic evolution characterized by Anabor et al. (2008) thus closely resembles the stages of a passing trough discussed in sections 5a and 5b.

North of the Sierras de Córdoba is an interesting feature seen as a precipitation maximum along the Andes foothills in the northern FHS area (Figs. 8a,f–h). This precipitation maximum coincides with a maximum in deep and wide convective cores in the evening (Figs. 9d and 10d, respectively) and wide convective cores and possibly broad stratiform regions at night (Figs. 10a and 11a, respectively). We are cautious about the latter because the number of broad stratiform regions in the FHS is small (Table 1). However, the time sequence of events suggests triggering and subsequent mesoscale development locally, without eastward propagation, possibly because this region is sufficiently equatorward of the westerlies.

2) DEEP CONVECTIVE CORES IN THE FHS AND PLB

Analysis of the diurnal cycle of the different echo categories in higher time resolution further clarifies the connection between the different radar echo structure types and the evolution of MCSs. Figure 12 shows the diurnal cycles for all three extreme echo structure categories determined from the TRMM PR for the FHS and PLB regions. To minimize possible sampling errors we applied a 4-h running mean to the diurnal cycle, as suggested by Negri et al. (2002a).

Deep convective cores in the FHS region occur most frequently in the late afternoon and evening hours (Fig. 12a). This peak is clearly related to the echoes in the Sierras de Córdoba (Fig. 9d). This region is where Zipser et al. (2006) found some of the deepest convection on Earth (Fig. 2b), and where severe storms and tornadoes are known to occur primarily from early afternoon to midnight (Altinger de Schwarzkopf and Rosso 1982). The diurnal cycle of the deep convective cores in the PLB region is similar to that in the FHS, except that the peak occurrence time is somewhat noisy (Fig. 12b). Deep convective cores in the PLB in the early afternoon are scattered over the whole region (Fig. 9c), probably as a result of diurnal heating. In the evening and early night they occur in the western part of the PLB region (Figs. 9a,d), likely associated with systems triggered in the FHS (over

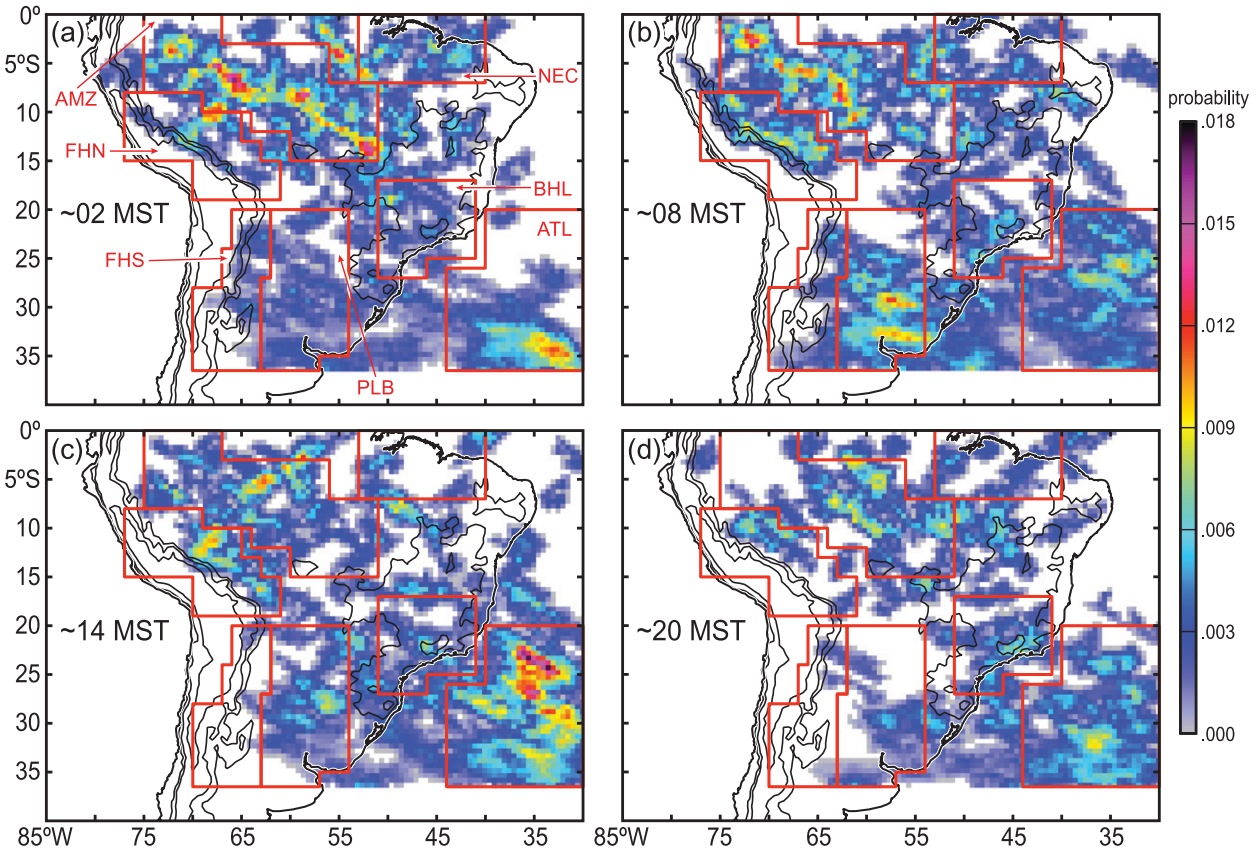

FIG. 11. As in Fig. 9, but for broad stratiform regions.

the Sierras de Córdoba in the FHS; see Fig. 5d) and subsequently advected eastward by the midlevel westerlies (Fig. 3b) into the PLB region. Both the scattered afternoon and orographically triggered evening deep convective cores contribute to the peak in Fig. 12b.

As noted in section 5a, synoptic-scale low-level moisture transport favors extremely deep convection in the FHS. The diurnal timing of the convection is related to the diurnal heating of the high terrain of the Andes and is determined by mechanisms that are responsible for lifting the low-level air to saturation to release its instability. Figure 13 shows the composite diurnal cycle of surface winds and divergence for days when deep convective cores occur in the FHS. The Andes are characterized by extreme divergence in the late night and morning (Figs. 13a,b) and pronounced convergence over the extremely high terrain from midday through evening (Figs. 13c,d). In the late afternoon and evening, this convergence over the high terrain draws low-level air from the east and northeast toward the Andes in the southern part of the continent. Some of this low-level air must pass over the sharply rising Sierras de Córdoba just upstream of the Andes, lifting the air over this range. A composite sounding for ~2000 MST at 35°S, 65°W (Fig. 12e) shows that the lower layer, below the strong westerlies, is conditionally unstable and rather dry. It requires ~2 km of lifting to release the instability. The Sierras de Córdoba comprise a continuous ridge that is just over 2 km in height, just enough to bring the low-level air to saturation and release intense convection in the late afternoon to early evening hours over the Sierras, upstream of the Andes.

3) WIDE CONVECTIVE CORES AND BROAD STRATIFORM REGIONS IN THE FHS

Wide convective cores in the FHS have a diurnal cycle of occurrence that is similar to that for the deep convective cores, but with a broader peak occurring about 4 h later (Fig. 12c). This similarity suggests that these two echo categories occur under similar conditions. Indeed, in the FHS area, there is an overlap of deep and wide convective cores of close to 20% of both categories combined, and the composites of wind and divergence data for these two echo categories in this region were almost identical. Therefore, we consider Fig. 13 as being representative for the wide convective cores as well. The

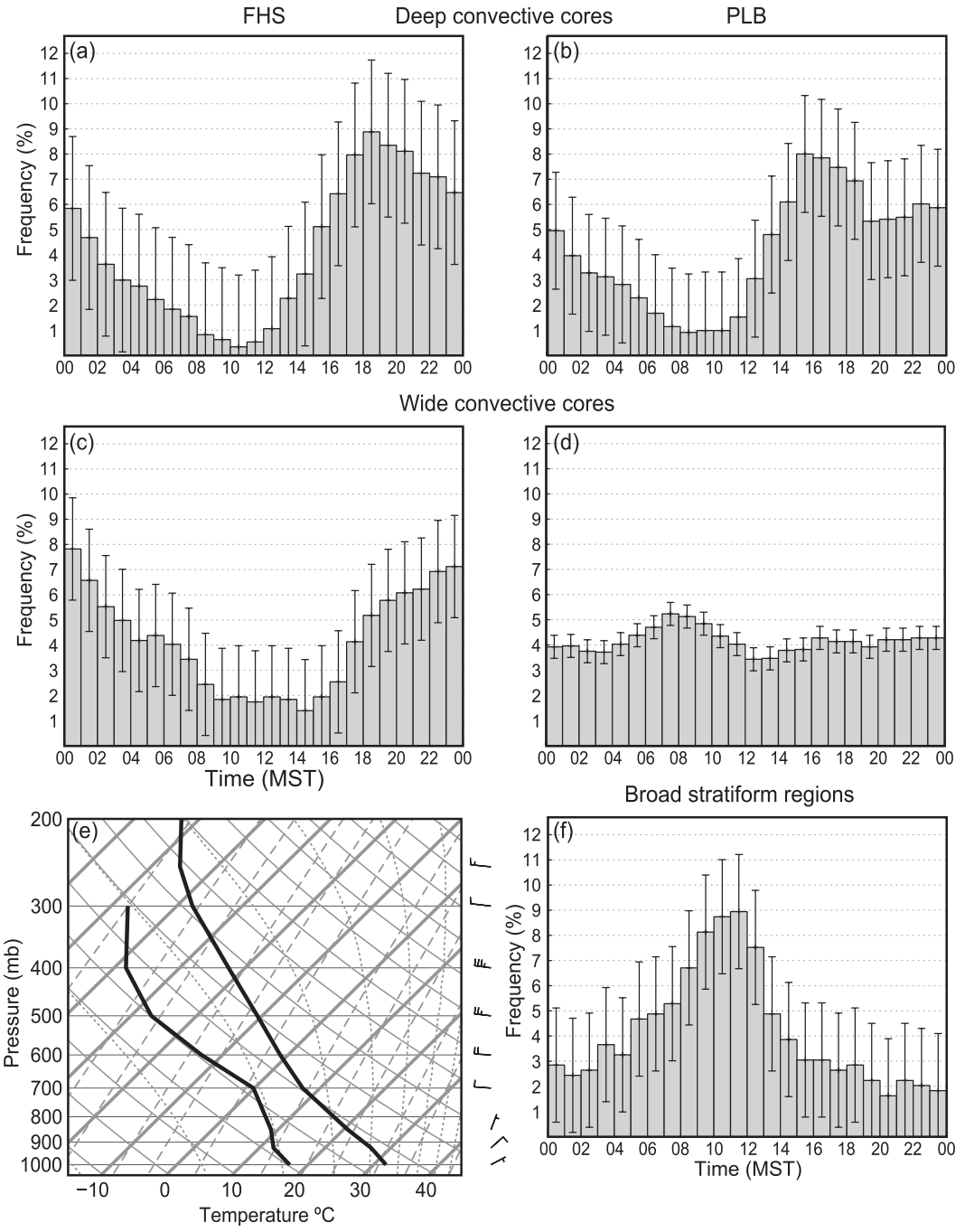

FIG. 12. Diurnal cycle of the frequency of occurrence of (a),(b) deep convective cores, (c),(d) wide convective cores, and (f) broad stratiform regions in the (left) FHS and (right) PLB regions. The RMS error is shown (black bars). (e) Sounding from NCEP–NCAR reanalysis composite fields for days when deep convective cores occurred in the FHS region extracted at 35°S, 65°W (white circle in Fig. 1b) at 0000 UTC (~2000 MST).

maximum occurrence of wide convective cores in the FHS region is from around midnight to 0100 MST. The composite wind pattern at about this time (Fig. 13a) indicates that the low-level flow into the FHS–PLB region at the time of maximum occurrence of wide convective cores has a more northerly component than in the early evening (Fig. 13c). It can thus be suggested that the convective systems that develop upscale to contain wide convective cores are more strongly fed moisture by the SALLJ. Broad stratiform regions represent a still later

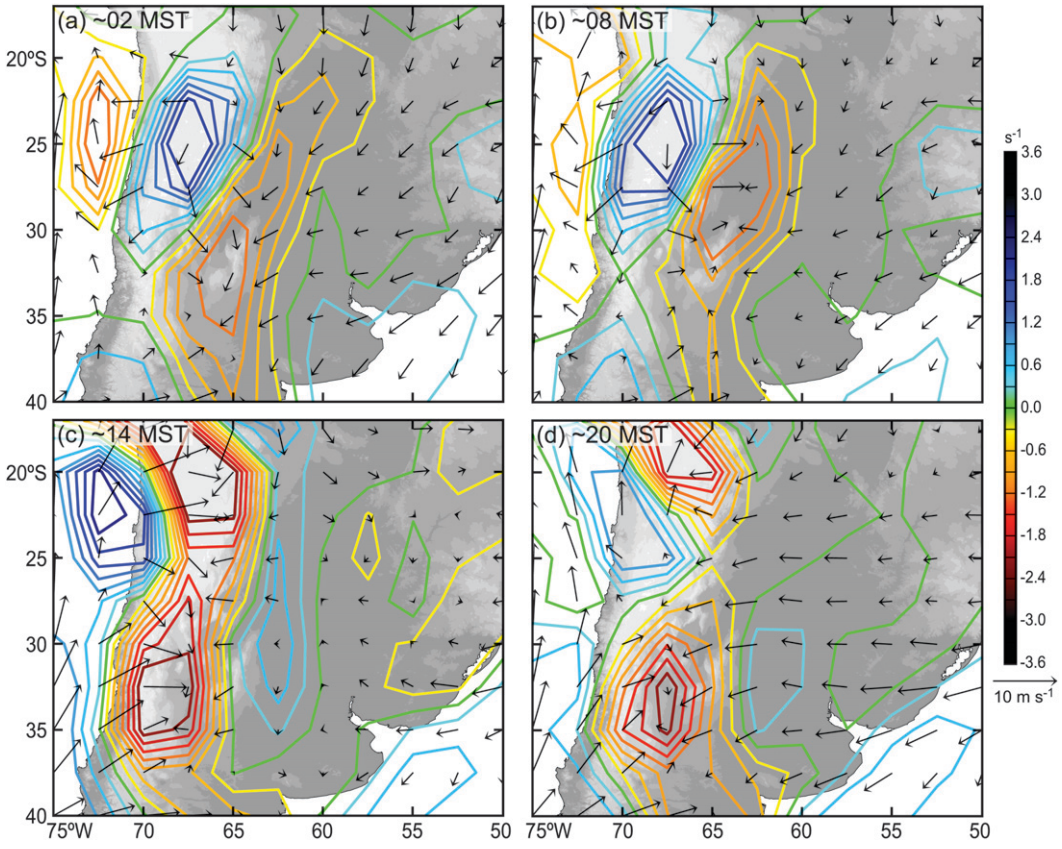

FIG. 13. NCEP–NCAR reanalysis surface winds (m s^{-1}) and divergence (s^{-1}) composites at (a) 0600 UTC (~0200 MST), (b) 1200 UTC (~0800 MST), (c) 1800 UTC (~1400 MST), and (d) 0000 UTC (~2000 MST) for days when deep convective cores were observed in the FHS region.

stage of MCS development, and the few broad stratiform regions that are observed in the FHS are consistent with this view in that they all occur in the late night to morning hours (not shown). However, the number of broad stratiform regions in the FHS (Table 1) is clearly too small to hold up for conclusions.

4) WIDE CONVECTIVE CORES AND BROAD STRATIFORM REGIONS IN THE PLB

Although the wind and divergence composites for the PLB echo structures (not shown) closely resemble those for the FHS region (Fig. 13), wide convective cores and broad stratiform regions in the PLB exhibit a diurnal cycle distinct from the deep and wide convective cores over the FHS (cf. left and right panels of Fig. 12). The wide convective cores in the PLB have a weak diurnal cycle, but nonetheless have a weak maximum frequency of occurrence at about 0600–1000 MST. The broad stratiform regions have a strong maximum frequency slightly later, beginning at about 0800 MST and cutting off sharply around 1200–1300 MST. This sequence is consistent with the further development of convective systems originating upstream over the FHS and evolving into broad MCSs out over the flat terrain of the PLB. Studies of MCSs (Salio et al. 2007) and MCCs (Velasco and Fritsch 1987) over southeast South America using IR satellite imagery show a maximum in the initiation of MCSs and MCCs in the afternoon and evening and the mature stage mainly during the night and early morning. Nogués-Paegle and Mo (1997) found a maximum in vertically integrated moisture flux for wet periods in this area between 0200 and 0800 LT, providing the necessary moisture to keep the convective systems growing at this time of day.

The upscale maximization of the broad stratiform region echoes at this time of day is further aided by the powerful diurnal cycle of heating and cooling over the Andes to the west. In the morning hours strong downslope flow associated with the strong nighttime divergence at the top of the Andes converges with the SALLJ (which is strongest at night) and other northeasterly and easterly surface flow over the PLB (almost identical to the patterns shown in Fig. 13b). This convergence aids in the development of broad stratiform regions in the later stages of the MCSs triggered in the late evening or

nighttime in the FHS or PLB regions. This inference agrees with conclusions of Nicolini and Saulo (2006), who found that stronger-than-normal wind convergence over the La Plata basin leads to the observed nocturnal precipitation maximum. The convergence sharply cuts off at midday, when heating over the Andes begins to draw the surface flow upward again (as in Fig. 13c). MCSs containing wide convective cores and broad stratiform regions in middle and late stages of their life cycle, respectively, are probably responsible for the nighttime–morning precipitation maximum seen over the La Plata basin in Figs. 8a–c,h, and described for this region by Kikuchi and Wang (2008).

b. *Control of extreme convection in the FHN by the diurnal heating cycle of the Andes*

The occurrence of extreme convection becomes more probable in the northern (tropical) portion of the Andes in the synoptic setting of the east coast trough regime (section 5b). In these conditions some extreme convection is closely tied to the Andes foothills in the FHN region (Figs. 5b,d). In this region, deep convective cores are rare (Fig. 9). However, wide convective cores and broad stratiform region echoes are observed, with peak frequency during the late night and morning (Figs. 10a,b, 11a,b, and 14a). During the afternoon and evening they occur farther off the mountains in the southwestern part of the Amazon basin. The peak in wide convective cores in the early afternoon (Fig. 14a) probably represents convection triggered by daytime solar heating (Figs. 10c,d). The larger peak in late night and early morning is due to echo structures that form along the Andes foothills, probably as the nocturnal low-level flow is lifted over the foothill ridges such as the Cordilleras Vilcabamba and Azul (Figs. 1a and 10a,b).

The diurnal cycle for the broad stratiform regions has one pronounced peak in the late morning (Fig. 14c). It corresponds partly to echo structures over the foothills and partly to echo structures located over the Amazon basin (Fig. 11c). The peak is observed after the peak in wide convective cores, again suggesting that they are part of similar MCSs in either an early, more convective, or later, more stratiform, stage of their life cycle. Note, however, that the number of broad stratiform regions in this region is relatively small (Table 1). It is interesting that although the afternoon and evening cold cloud fraction observed in IR data over the crest of the Andes is larger than that during the late night and morning at the foothills (Garreaud and Wallace 1997), the late night and morning convective systems produce a much larger amount of precipitation (cf. Figs. 8b,f).

As mentioned above, we suggest that orographic lifting of the north-northwesterly low-level flow (Fig. 3d) at the foothills accounts for increased convective activity and precipitation as proposed by Lenters and Cook (1995). The question remains as to why this mechanism is only effective during the night. A diurnal composite analysis of the surface winds and divergence for days when wide convective cores are observed in the FHN (Fig. 15) reveals massive daytime heating over the mountain crests and plateaus, especially the Altiplano, leading to extreme convergence of the surface winds at mountaintop level (Figs. 15c,d). Upslope winds in response to the heating probably transport moisture to high elevations, leading to the observed afternoon and evening convection and precipitation over the Altiplano (Figs. 9c,d and 8f,g, respectively). While the mountaintop heating forces surface winds upslope, it also creates a strong divergence zone along the foothills, preventing convection there. During the night and morning, cooling over the mountain tops reverses these mechanisms, and convergence is restored at the base of the Andes (Figs. 15a,b).

Romatschke et al. (2010) found a similar late night to early morning maximum in wide convective cores along the Himalayan foothills during the South Asian monsoon. The mechanisms leading to this maximum were similar to those described here; however, because of the extreme nocturnal cooling of the Tibetan Plateau they even found nocturnal downslope flow converging with the prevailing moist monsoon flow over the plains. We speculate that such downslope winds converging with the moist flow from the Amazon basin might be present along the Andes foothills, as suggested by Giovannettone and Barros (2009), although they are not clearly resolved in the NCEP–NCAR reanalysis data.

c. *Extreme convection over the AMZ comes from two directions, merges, and takes the form of nocturnal broad stratiform regions*

Extreme convection in the AMZ region generally occurs in the synoptic setting of the east coast trough regime (section 5b), although, as discussed in section 5b, the synoptic forcing seems to play a less important role than in other regions, for example, the FHN. The AMZ and NEC regions exhibit a much different form of extreme convection than that which occurs in the FHN. In particular, the extreme convection over the AMZ region is not as strongly controlled by mountainous topography.

Convection in the AMZ region, as represented by the diurnal precipitation climatology, starts in the early afternoon as two northwest–southeast-oriented lines of maximum rainfall (Fig. 8e). Convection in these two bands produces maxima in cold cloud coverage in IR imagery (Garreaud and Wallace 1997) and is therefore likely deeper than convection at later times. However, the convective cells are not deep enough to be captured by

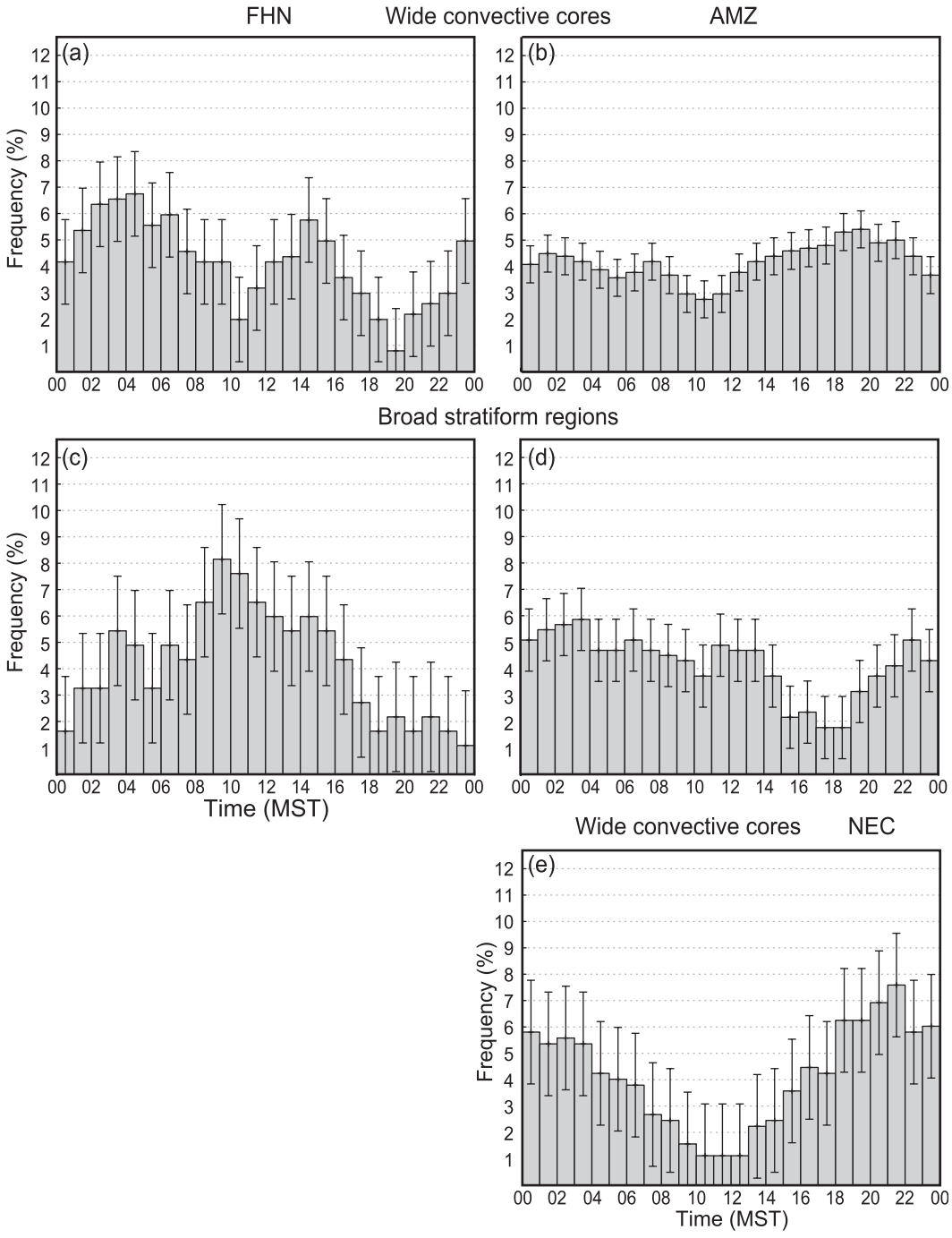

FIG. 14. Diurnal cycle of the frequency of occurrence of (a),(b),(e) wide convective cores and (c),(d) broad stratiform regions in the (a),(c) FHN and (b),(d) AMZ and (e) NEC regions. Black bars show the RMS error.

the deep convective core category (Fig. 9c). The early afternoon northwest–southeast-oriented precipitation bands do, however, coincide with the occurrence of systems with wide convective cores (Fig. 10c). In the late afternoon, the two lines merge and the convection spreads out to cover the Amazon basin (Fig. 8f). Wide convective cores occur with roughly similar frequency throughout the day, but the late afternoon merger of precipitation bands seen in Fig. 8f corresponds to the slight uptick in occurrence of wide convective cores in the late afternoon (Fig. 14b). Negri et al. (2000, on their page 52) describe this phenomenon as analogous to waves in a string that is

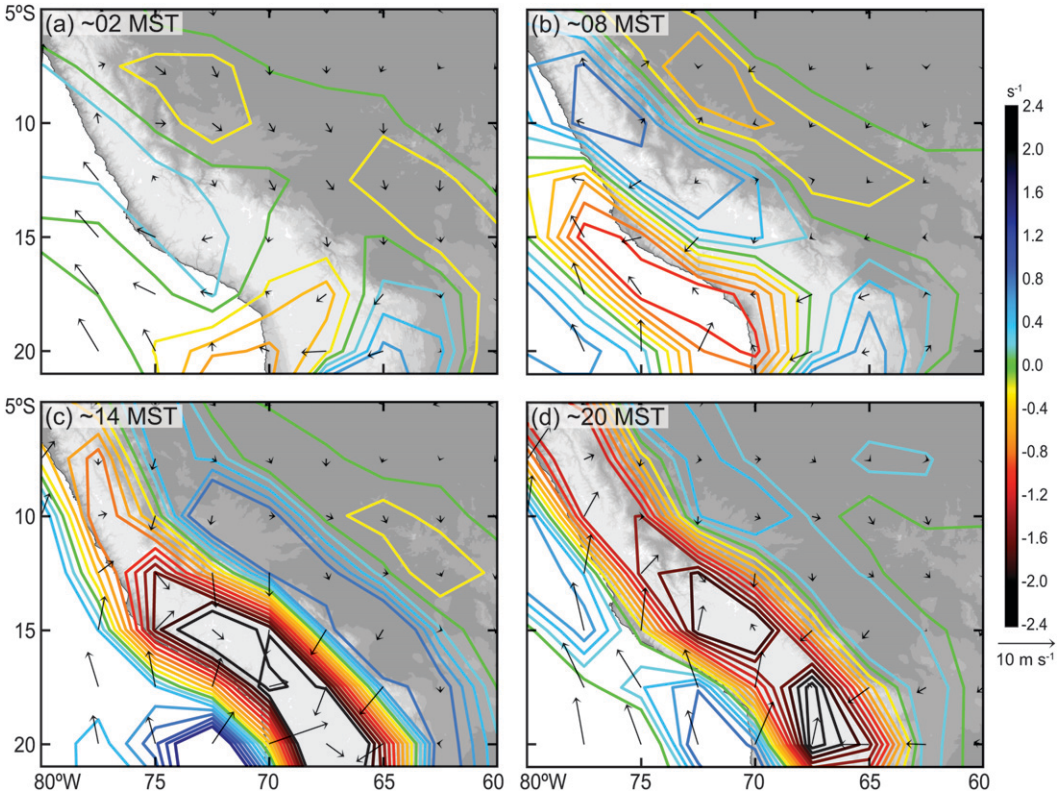

FIG. 15. As in Fig. 13, but for wide convective cores in the FHN region.

fixed at both ends, the ends in this case being the Andes in the southwest and the northeastern coast (see section 6d). They describe that "Both ends generate convection that propagates into the Amazon Basin, initiating new convection, and interacting with convection initiated within the basin itself, all apparently complicated by the effects of the rivers."

At the location where the two northwest–southeast lines of precipitation merge, a line of maximum precipitation forms and persists throughout the night (Fig. 8a–c, g,h). The frequency of broad stratiform regions reaches a maximum for several hours, around 0300 MST (Fig. 14d). This sequence, in which the maximum occurrence of broad stratiform regions comes several hours after the maximum of wide convective cores, again points to a likely evolution of MCSs with embedded wide convective cores evolving into systems containing broad stratiform regions at later times. The time of maximum occurrence of broad stratiform regions is consistent with results of Machado et al. (2004), who found the maximum total cloud cover during the night over Brazil. Negri et al. (2002b) showed a lag of 2 h between the maxima in convective and stratiform rain rates.

The maximum of occurrence of broad stratiform region echoes at ~0200 MST falls along a northwest–southeast line in the AMZ region (Fig. 11a). This line coincides with the northwest–southeast line of maximum precipitation persisting throughout the night (from ~2000 to ~0800 MST in Fig. 8), which formed from the merger of the two lines of precipitation existing earlier in the day, and which was most pronounced at about 0200 MST (Fig. 8a). This line also coincides with the northwest–southeast band that constitutes the maximum overall seasonal precipitation across northern South America (Fig. 2a). This three-way coincidence of northwest–southeast lines indicates that the MCSs that develop broad stratiform regions over the AMZ are important contributors to the overall summer season precipitation in the Amazon region.

By applying an empirical orthogonal function analysis to TRMM data, Kikuchi and Wang (2008) found an area-wide daytime precipitation maximum over the Amazon region. Figures 8e,f show that the daytime precipitation is generally widespread over the region, but actually has a relative minimum in a northwest–southeast zone located between the two bands discussed above. However, this minimum is where Fig. 2a shows the seasonal accumulation to be greatest. We infer, therefore, that the nocturnal systems with broad stratiform regions, which maximize along the northwest–southeast line seen in

Fig. 11a, account for the northwest–southeast-oriented seasonal maximum in Fig. 2a, when added to the daytime maximum convective systems. Some individual locations along the nocturnal precipitation band actually have an overall nocturnal precipitation maximum; for example, the city of Humaitá, Brazil, located along the nocturnal precipitation band at 7.5°S, 63.0°W on the bank of the Rio Madeira has a clear precipitation maximum after midnight (Angelis et al. 2004). Negri et al. (2002b) conducted a high temporal and spatial resolution analysis of the diurnal cycle of precipitation in the Amazon basin. Close inspection of their maps also reveals nighttime maxima along the Amazon and neighboring rivers and daytime maxima in the surrounding areas. The highly local role of the rivers in favoring the nighttime maxima associated with broad stratiform regions is curious and a topic for further study.

The northwest–southeast-elongated precipitation area over the AMZ, which persists throughout the night, is associated with larger-scale wind convergence. Easterly winds from the Atlantic turn south at the Andes and become the northwesterlies observed at the 700-mb level along the eastern Andes foothills (Fig. 3c), converging with the easterly flow from the Atlantic. The convergence seen in the NCEP–NCAR winds is increased in the evening hours (not shown) at the time of the evening merger (Fig. 8g) of the two lines of convection, which were observed in the early afternoon (Fig. 8e), into one single line of convection. The increase of wide convective cores in the evening (Fig. 14b) and the maximization of broad stratiform regions during the night (Figs. 11a and 14d) might be related to this peak of convergence in the region.

The TRMM data indicate further details of the complex diurnal variability in the AMZ region. Comparison of Figs. 8e,1 indicates that the first afternoon convection in the southeastern Amazon basin is triggered over the lower terrain (above 250 m) of the Brazilian Highlands. Laurent et al. (2002) show triggering over the terrain around the location of the TRMM-LBA field campaign region (~6° to ~16°S, ~56° to ~66°W), which is located within the southern line of early convection (Fig. 8e). Most of their observed MCSs were initiated over terrain between 200 and 300 m. Diurnal heating over the slightly elevated terrain plus the moisture supply of the Amazon rain forests probably combine to set ideal conditions for the triggering of convection in this region. One exception to the early triggering over elevated terrain is the early afternoon precipitation maximum observed at ~4°S, 61°W (Fig. 8e), which is located over the lowlands. It corresponds to a maximum in broad stratiform regions (Fig. 11c) and occurs over a region with a strong underlying moisture source, where the Rio Negro joins the Amazon River. Wide convective cores and a corresponding precipitation maximum are observed in the preceding hours moving in from the northeast (Figs. 10b and 8a–d,h) as discussed further in section 6d. The MCSs containing these wide convective cores probably form large stratiform regions later in their life cycle, which are observed as broad stratiform regions in the early afternoon (Fig. 11c). We speculate that the presence of these daytime-maturing MCSs together with the solar heating and underlying moisture source contribute to the observed precipitation maximum in the early afternoon (Fig. 8e).

The spreading out of precipitation to the northwest in the afternoon (Figs. 8e–f) is likely at least in part due to convection triggered by solar heating, which takes longer to form without the enhanced heating over elevated terrain. It might also be convection triggered by cold outflow from previous convective cells. Cifelli et al. (2002) studied two MCSs from the TRMM-LBA campaign data during different synoptic conditions. One formed as a squall line and was triggered by cold outflow from previous convection to the northwest (Amazon squall lines are discussed further in section 6d). The other MCS formed by convective cells merging together after they were probably triggered by solar heating, suggesting that both mechanisms play a role in the spreading of the convection to the northwest.

Machado et al. (2002), who studied IR data over the core of the TRMM-LBA region (9.8°–12.1°S, 61.0°–63.3°W), found high cloud fractions for lower brightness temperature thresholds, associated with deeper convection, in the late afternoon and for higher thresholds during the late night and early morning hours, consistent with the evolution of MCSs. They also show the evolution of the typical sizes of the convective systems as increasing during the afternoon, with maximum extent during the evening, and slightly smaller scales persisting through the night. When generalized over a larger area, IR data with temperatures below a certain threshold show the largest area expansions of convective systems over the Brazilian Highlands in the early afternoon and over the northwestern Amazon basin in the later afternoon (Machado and Laurent 2004). This result agrees with our findings of convection starting first in the southeast and then spreading to the northwest. The broad stratiform regions observed during the night, which correspond to a maximum in overall precipitation (Fig. 2a), however, are not evident in IR brightness temperature data (Machado and Laurent 2004).

d. Squall lines form in the NEC and move into the Amazon region

It is known from earlier work (Garstang et al. 1994; Kousky and Molion 1981; Molion 1987) that intense and

areally extensive squall-line MCSs form in the northeast coastal zone of South America, in response to daytime maximum of convergence, where the easterlies coming from the Atlantic slow down over the continent. This profound coastal convergence zone is evident in the NCEP–NCAR winds in Figs. 4c,d. Garstang et al. (1994) analyzed three mesoscale to synoptic-scale squall-line systems, which they describe (on their page 608) to be ''among the most important rain producers in the rain forests of the central Amazon Basin.'' The systems were composed of merged convective cells triggered during the afternoon in a sea-breeze convergence zone along the northeast coast of South America. The line-shaped areas of convection, reaching total lengths of over 3000 km, moved southwest at speeds of 14–17 m s^{-1} with the low- to midlevel winds. The squall lines weakened during the night but were reinforced during the time of maximum diurnal heating near the location of the northern line of early convection described above. Some of these squall lines are persistent enough to reach the western boundaries of the Amazon basin. Rickenbach (2004) observed squall lines originating from the northeast coast in the TRMM-LBA campaign region that caused a secondary nocturnal precipitation maximum. Salio et al. (2007) found nocturnal MCSs associated with squall lines originating at the Brazilian coast in the southern parts of tropical South America.

The diurnal statistics of TRMM PR radar echo structures and precipitation are consistent with these earlier studies of squall lines generated diurnally in the northeastern coastal convergence zone. The location of the first extreme convection in the afternoon is along the eastern sides of the mouths of the Amazon River and the Rio Tocantins (Figs. 1, 9d, 10c–d, and 8e–f). The time of day of the triggering suggests that heating of the landmasses and a local sea breeze combine with the synoptic-scale convergence in the coastal region, and with moisture supplies of the river deltas to initiate convection as suggested by Negri et al. (2000). Note that very little convection is found over the eastern end of the continent where the wind convergence at the surface (Figs. 4c,d) is counteracted by divergence at the 700-mb level (not shown) and the air is drier, unlike the saturated conditions over the mouth of the Amazon.

The extreme convective storms that form in the coastal convergence zone within the zone of maximum afternoon precipitation (Figs. 8e,f) move inland during the night. This southwestward movement is evident in the diurnal precipitation pattern [Figs. 8a–d,g,h; see also Negri et al. (2002b)]. This line-shaped zone of maximum precipitation loosely coincides with extreme convection in the form of wide convective cores moving farther inland (Figs. 10a,c,d). The diurnal cycle of the wide convective cores (Fig. 14e) reflects the afternoon triggering and southwest movement of the line of extreme convection by showing an increase in wide convective cores in the NEC during the afternoon, a maximum in the evening, a decrease in the early morning, and a minimum around noon, when the line of convection has weakened and moved out of the NEC region.

e. Deep and wide convective cores are released when Atlantic air is diurnally forced upward over the BHL

The diurnal cycles of the occurrence of deep and wide convective cores in the BHL region peak strongly in the afternoon. The peak in deep convective cores is stronger than in any other region (Fig. 16a). The peak in wide convective cores is similar but it extends until midnight (Fig. 16c), suggesting that early convective systems containing deep convective cores merge and form systems containing wide convective cores, as was seen to occur also in the FHS (section 6a). In this region, though, there is less of a tendency for the systems to develop further upscale, as evidenced by the occurrence of broad stratiform regions being relatively infrequent with no particular diurnal preference (Figs. 11 and 16e; Table 1). Divergence anomaly composites for days with broad stratiform regions observed in the BHL show stronger-than-average convergence during all times of the day (Fig. 17), suggesting that—unlike the strongly diurnally forced deep and wide convective cores—synoptic forcing is more important than diurnal/topographic forcing for the formation of broad stratiform regions in this region (see also section 5b). However, this inference is tentative because the total number of observed broad stratiform regions is relatively small (Table 1).

The strongly diurnally forced extreme convection in the form of deep and wide convective cores in the BHL occurs mainly along the coast of the southern Brazilian Highlands (Figs. 9c,d and 10c,d) in a region of strong surface wind convergence. Figure 18c shows the composite wind and divergence for days with deep convective cores in the BHL; composites (not shown) for days with wide convective cores occurring in the BHL show similar results. This convergence is likely a result of the strong diurnal heating over the Brazilian Highlands, which not only leads to a sea-breeze effect on the eastern side but also to westerly winds on the western side of the Brazilian Highlands. A sounding for ~1400 MST at 22.5°S, 47.5°W extracted from the composites for the deep convective cores (Fig. 16b) shows that the easterly winds at the coast are only present in the lowest levels. Westerlies occur at and above 700 mb. This

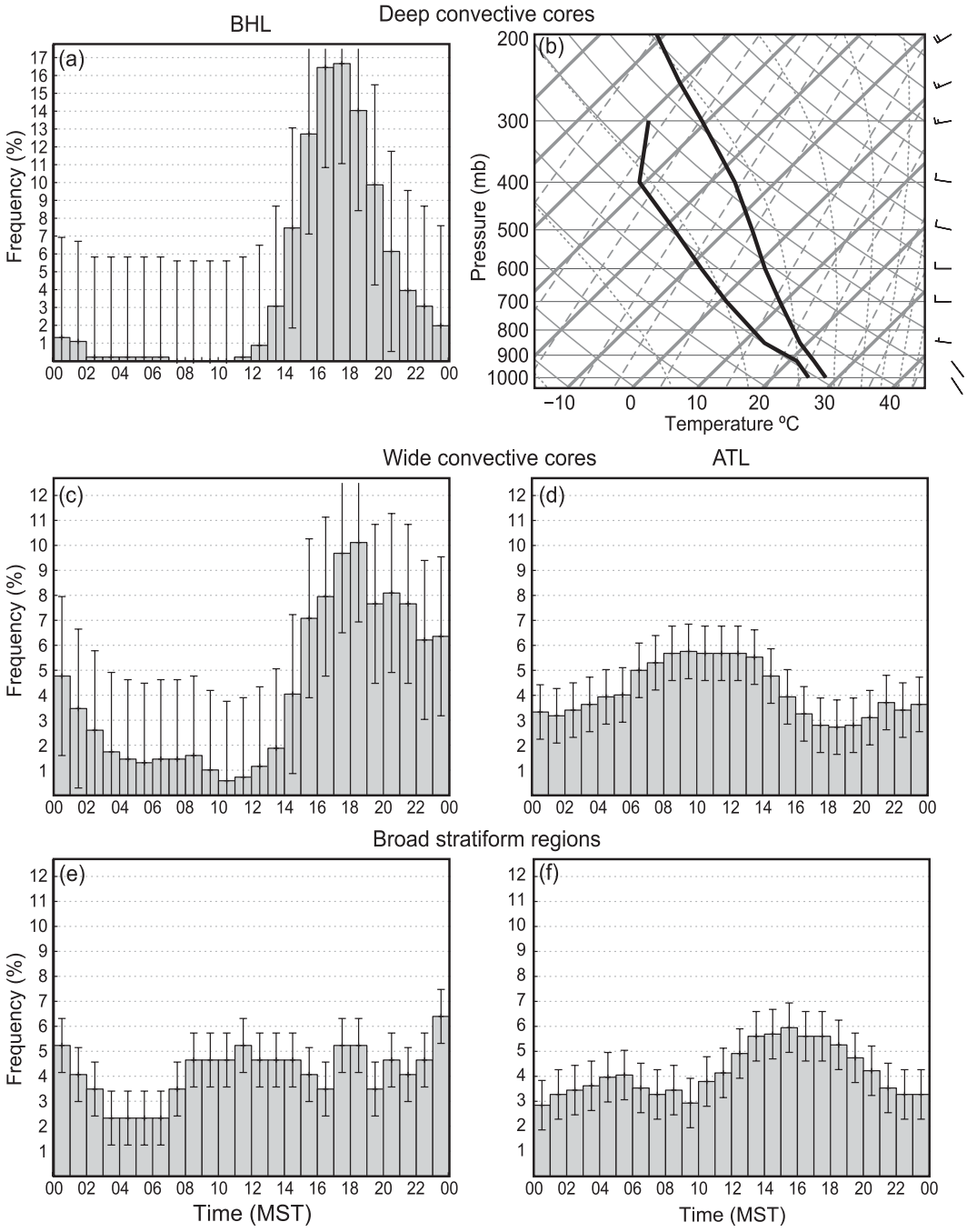

FIG. 16. Diurnal cycle of the (a) frequency of occurrence of deep convective cores, (c),(d) wide convective cores, and (e),(f) broad stratiform regions in the (left) BHL and (right) ATL regions. The RMS error is shown (black bars). Note the different scale in (a). (b) Sounding from NCEP–NCAR reanalysis composite fields for days when deep convective cores occurred in the BHL region extracted at 22.5°S, 47.5°W (white diamond in Fig. 1b) at 1800 UTC (~1400 MST).

strong directional wind shear produces similar conditions to those over the FHS region [sections 5a and 6a(2)] with moist low-level air, in this case from the Atlantic, being overridden by dry upper-level air from the continent. This allows strong instability to build up, which is released either by sea-breeze convergence or when the moist low-level flow is lifted over the coastal mountains and over the Brazilian Highlands.

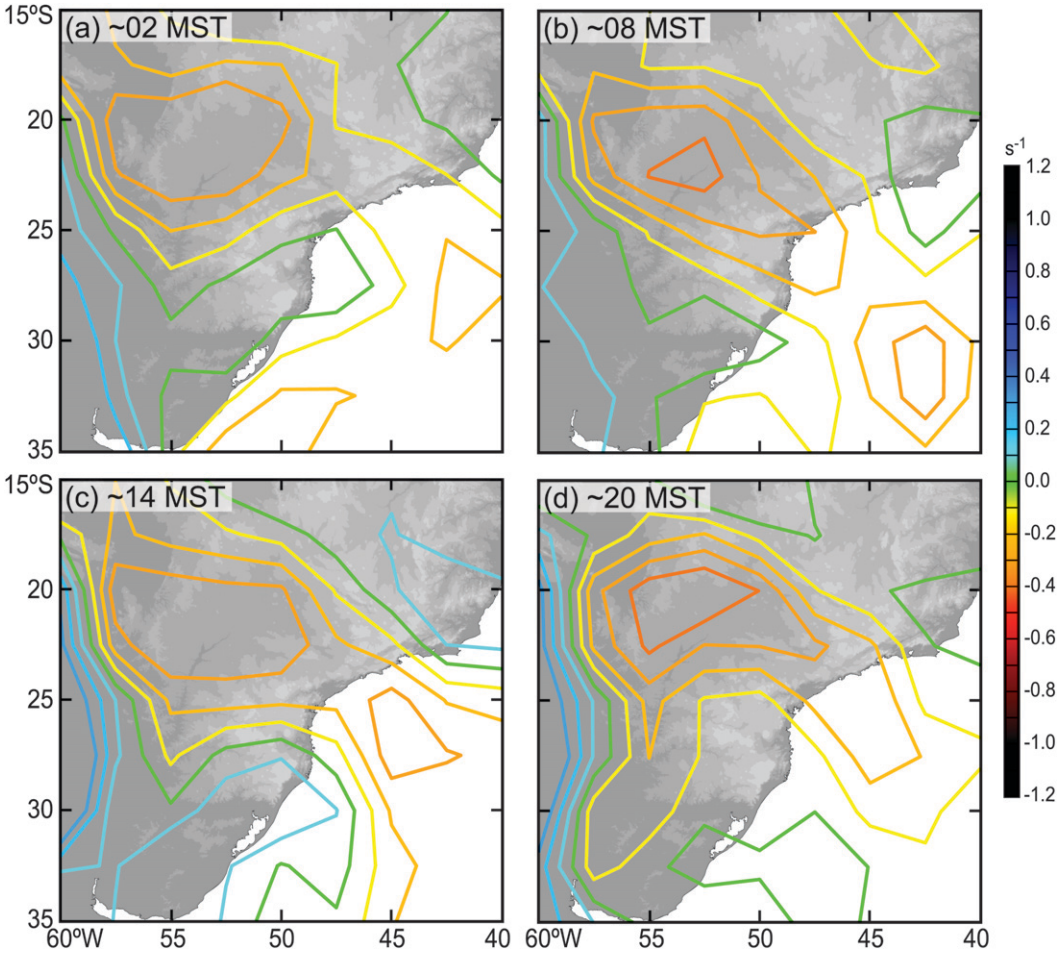

FIG. 17. NCEP–NCAR reanalysis surface divergence anomaly (s^{-1}) composites at (a) 0600 UTC (~0200 MST), (b) 1200 UTC (~0800 MST), (c) 1800 UTC (~1400 MST), and (d) 0000 UTC (~2000 MST) for days when broad stratiform regions were observed in the BHL region.

f. Wide convective cores and broad stratiform regions form over the ATL with a diurnal cycle related to heating over the continent

Convection in the oceanic part of the SACZ is enhanced in the synoptic setting of the Atlantic trough regime (section 5c). However, the intensity of the oceanic SACZ is not only influenced by the synoptic regime but also by the diurnal heating over the South American continent. Diurnal composites of surface wind and divergence patterns for days when wide convective cores (Fig. 19) occur do not indicate any significant diurnal variation in the amount of low-level convergence over the ATL, except at ~2000 MST, when the convergence is somewhat weaker. Composite maps for days when broad stratiform regions are observed are similar to those in Fig. 19 and are not shown. The weakening occurs at the time of day when the pronounced diurnal convergence over the high Andes terrain is strongly drawing Atlantic air landward toward the mountains (Fig. 19d). The easterly landward component of the surface wind weakens the convergence over the Atlantic. The time of this effect (~2000 MST) coincides with a minimum in wide convective cores (Fig. 16d) and a decrease in broad stratiform regions (Fig. 16f). During the night, the undisturbed wind pattern is slowly rebuilt leading to a strengthening of the convergence over the Atlantic and an increase in wide convective cores in the morning (Figs. 9c and 16d). The broad diurnal peak of occurrence of wide convective core echoes at ~0700–1300 MST (Figs. 10b,c and 16d) is followed by a maximum occurrence of broad stratiform regions a few hours later, at ~1300–1900 MST (Figs. 11c,d and 16f). This time lag indicates that extreme convection over the ATL takes the form of MCSs with wide convective cores in their earlier stages and developing broad stratiform regions in their later stages. As already mentioned (section 4b), deep convective cores rarely occur over the ATL (Fig. 9).

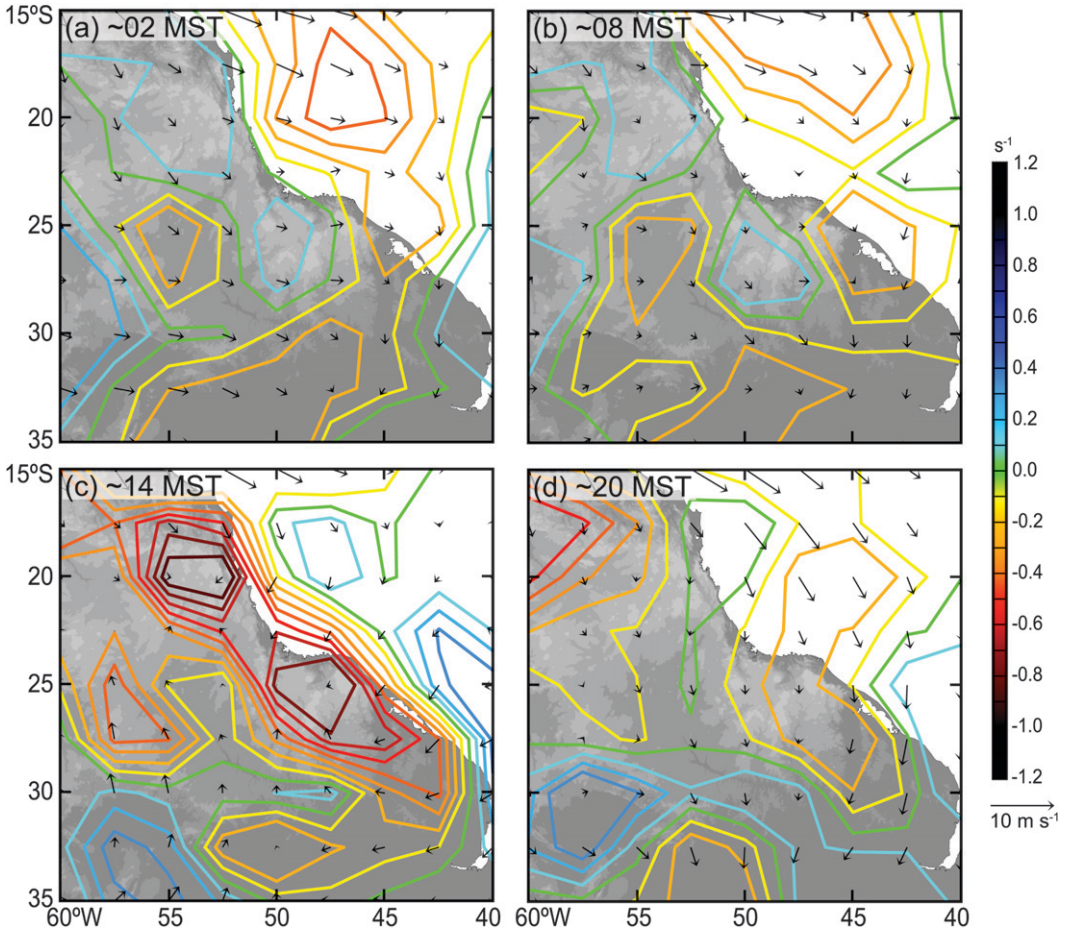

FIG. 18. As in Fig. 13, but for deep convective cores in the BHL region.

Another process may be involved in determining the peak of occurrence of MCSs, with wide convective core echoes in the morning over the ATL. Mapes et al. (2003) noted that the extreme daytime heating over the elevated Andes terrain can generate a mesoscale gravity wave that propagates away from the mountains and triggers MCSs at a distance from the Andes during the morning. They noted this process over the Pacific west of the tropical Andes. We wonder if it is not possible that a similar wave could propagate eastward from the subtropical Andes and excite convection over the ATL in the morning hours.

7. Conclusions

Analysis of the summer months of 10 yr of TRMM PR data has shown how the effects of daytime solar heating and forcing by the topography combine with different synoptic scenarios to trigger and develop a variety of particularly intense convective systems over the South American continent and the neighboring Atlantic Ocean. Three types of radar echo structures have been classified according to their 3D properties and convective/stratiform nature: *deep convective cores* (contiguous convective reflectivity values $\geq$40 dBZ, extending $\geq$10 km in height), *wide convective cores* (contiguous convective reflectivity values $\geq$40 dBZ, extending over an area of $\geq$1000 km^2 when projected on a horizontal plane), and *broad stratiform regions* (contiguous stratiform radar echoes, extending over an area of $\geq$50 000 km^2 when projected on a horizontal plane).

South America extends meridionally across many latitudes, and the climatology in our region of interest varies from tropical in the north, centered on the Amazon basin, to subtropical in the south, centered on the La Plata basin. Both climatological regimes are bounded on the west by the Andes. The South American low-level jet (SALLJ) connects the two regimes by advecting tropical air into the southern subtropical region. The strength of the SALLJ waxes and wanes with the passage of synoptic-scale waves in the westerlies. When a wave trough is over the Andes or the La Plata basin (i.e., the west

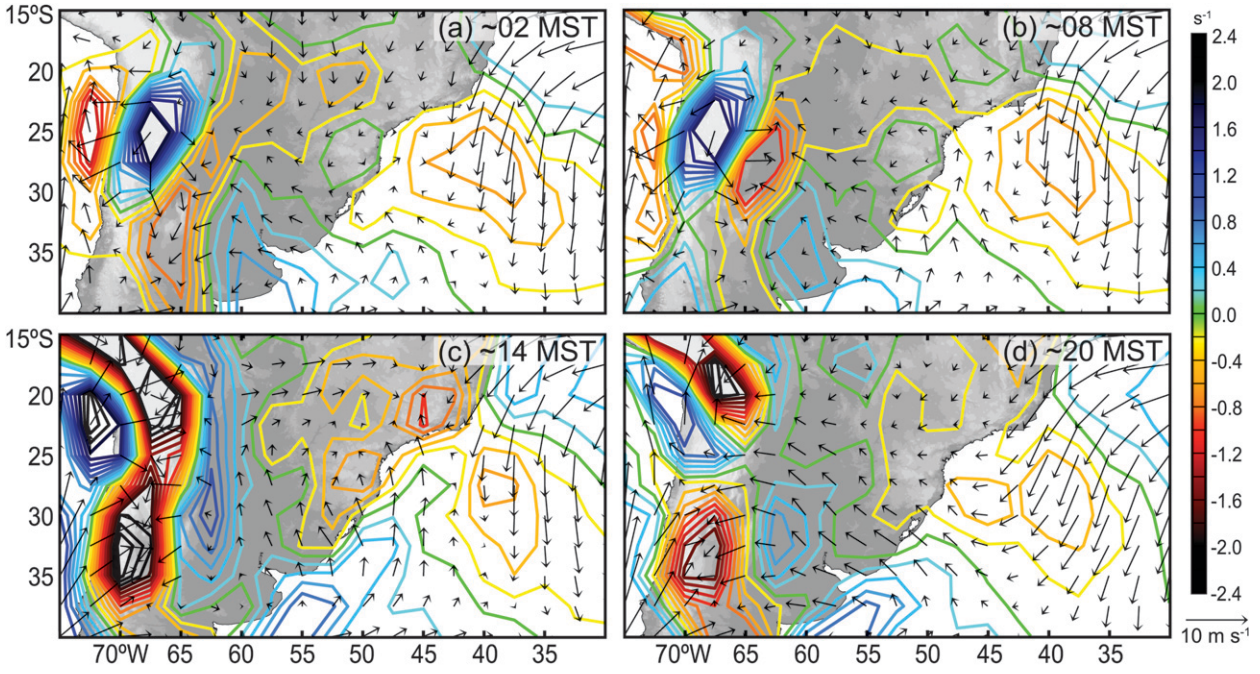

FIG. 19. As in Fig. 13, but for wide convective cores in the ATL region.

coast or La Plata basin trough regime), the SALLJ intrudes into the south and contributes to the formation of extreme convection over the southern foothills of the central Andes and over the La Plata basin. As the trough moves eastward (i.e., the east coast trough regime), surface high pressure builds over the La Plata basin and the SALLJ withdraws to the north, and extreme convection occurs on the tropical northern foothills of the central Andes. Extreme convection over the greater Amazon region, east of the Andes, is also associated with the east coast trough regime. However, because there is little synoptic variability in this region with different synoptic regimes, we conclude that the influence of the synoptic environment on the convection in this region is limited. When the trough moves over the ocean and deepens (i.e., the Atlantic trough regime), extreme convection occurs over the ocean, offshore from the Brazilian Highlands.

The frequency of occurrence of and form taken by extreme convection within the broader synoptic environments of both the northern tropical and southern subtropical/midlatitude zones is strongly modulated regionally by topography and the diurnal heating cycle.

In the FHS and PLB regions, all three types of extreme radar echo structures have strong maxima in their frequency of occurrence. Deep and wide convective cores have a maximum frequency in the FHS in the afternoon and evening in an environment of strong directional wind shear, in which moist easterly low-level flow is overridden by dry westerlies aloft. This sheared, moisture-stratified environment builds up strong instability, which is released as the low-level flow is lifted over the lower slopes and foothills of the Andes. The TRMM statistics indicate that the convective systems containing deep and wide convective cores propagate to the north and east over the wider La Plata basin during the night where they evolve to contain broad stratiform regions in the morning. This enhanced convective activity over the La Plata basin during the night and morning hours leads to a morning precipitation maximum in the PLB. The nocturnal convection is reinforced as downslope flow from the Andes (a result of nocturnal cooling over the mountains) converges with northerly low-level flow along the eastern Andes foothills, that is, the stronger-than-normal SALLJ ahead of a midlatitude wave passage.

In the FHN, extreme convection is associated with the later stages of midlatitude wave passages. The SALLJ does not extend to the subtropics in these synoptic conditions, shutting down the moisture transport to the subtropics. Instead, the tropical part of the nocturnal SALLJ impinges on the northeastern foothills of the central Andes, leading to maximum occurrence of wide convective cores at night, broad stratiform regions in the morning, and maximum precipitation from midnight to noon. Strong daytime convergence over the crests of the Andes, a result of daytime solar heating, leads to divergence along the foothills in the afternoon, preventing convection and precipitation at the base of the foothills during that time of the day.

In the AMZ region, precipitation is first observed in the early afternoon in two parallel bands extending from the northwest to the southeast. It is mostly triggered over elevated terrain in the eastern parts of the Amazon basin and partially in the western Brazilian Highlands. The precipitation bands are loosely associated with maxima in extreme echoes in the form of wide convective cores. Deep convective cores are rare in the AMZ. As a result of large-scale wind convergence, the two bands merge in the evening forming one broader band of precipitation right between the two original bands. This merger band persists throughout the night and coincides with a strong maximum in broad stratiform regions and also with the overall precipitation maximum in this region. Thus, although precipitation tends to peak in the afternoon over the Amazon basin as a whole (Kikuchi and Wang 2008), the nocturnal broad stratiform regions are implicated here in determining the exact location of the precipitation accumulation maximum.

In the NEC region, a climatological band of maximum precipitation forms along the coast, probably as a response to diurnal heating and a sea-breeze effect in combination with the moisture supply by major river deltas. This precipitation band moves farther inland with the prevailing northeasterly winds, weakens during the night, and becomes reinforced by solar heating at the location of the northern band of early precipitation in the AMZ region mentioned above. This precipitation band loosely corresponds to a maximum in wide convective core echoes and is likely associated with robust coastal squall lines described by Garstang et al. (1994).

In the BHL region, deep and wide convective cores are observed in the afternoon in a similar environment of strong directional wind shear as the daytime radar echo structures in the FHS region. The afternoon low-level sea breeze is overridden aloft by dry westerlies, which again lead to a build up of instability that is released as the low-level flow drawn inward by heating over the continent is lifted over the coastal mountains. The occurrence of systems with broad stratiform regions in the BHL did not show a strong diurnal cycle and thus did not have any preferred temporal relationship to the times of peak occurrence of deep and wide convective cores.

In the ATL region, deep convective cores are extremely rare if not completely absent. This behavior is consistent with other oceanic regions (e.g., Romatschke et al. 2010). Wide convective cores and broad stratiform regions do occur frequently and are associated with the passage of midlatitude waves off the continent. Low pressure over the eastern South Atlantic then leads to convergence enhancing the oceanic part of the SACZ. Large-scale convergence weakens in the evening, as a result of heating over the Andes drawing surface winds landward. A minimum of wide convective core formation occurs at this time, and broad stratiform regions shut off. As the convergence builds back up over the ocean in the ensuing hours, wide convective cores reach a maximum occurrence in the morning followed by a midday maximum of broad stratiform region occurrence. When the convergence weakens again later in the day, the cycle repeats.

The fact that wide convective cores peak after the deep convective cores in the FHS and BHL regions, and the broad stratiform regions peak after the wide convective cores in all regions but the BHL, suggests that the convective systems containing the different types of radar echo structures are not independent of each other. Systems containing deep convective cores likely organize upscale to contain wide convective cores at a later time in regions where both are present. The close relation of wide convective cores and broad stratiform regions, at a time lag of a few hours, indicates that they are both part of the same type of extremely large MCSs at different stages of development. These MCSs are known to be main producers of precipitation; therefore, it is not surprising that regions with maximum occurrence of wide convective cores and broad stratiform regions coincide with regions of maximum precipitation.

While the TRMM PR data provide a strong statistical dataset that allows the construction of a climatology such as that presented here, they remain limited by the orbital geometry that provides a limited number of snapshots per day at a given location. Moreover, the overpass timing is different over the northern and southern portions of the longitudinally extensive continent of South America. To further understand the behavior of extreme convection over this continent, we suggest that case studies of temporally continuous datasets documenting events in the different regions identified here would provide life history information that can only be surmised from the TRMM data. These case studies, moreover, should be supported by high-resolution model simulations of the events, such as have been done by Medina et al. (2010) for the South Asian region.

Acknowledgments. We acknowledge Stacy Brodzik for her assistance in processing the data used in this study. Carol Archambeault from NASA provided the TRMM PR data. NCEP–NCAR reanalysis data were provided by the NOAA/OAR/ESRL/PSD, Boulder, Colorado, (online at http://www.cdc.noaa.gov/). Beth Tully edited the manuscript and designed the graphics. This research was supported by the National Science Foundation under Grants ATM-0505739 and ATM-0820586 and by the National Aeronautics and Space Administration under Grants NNX07AD59G and NNX10AH70G.

REFERENCES

Altinger de Schwarzkopf, M. L., and L. C. Rosso, 1982: Severe storms and tornadoes in Argentina. Preprints, *12th Conf. on Severe Local Storms,* San Antonio, TX, Amer. Meteor. Soc., 59–62.

Anabor, V., D. J. Stensrud, and O. L. L. de Moraes, 2008: Serial upstream-propagating mesoscale convective system events over southeastern South America. *Mon. Wea. Rev.,* **136,** 3087–3105.

Angelis, C. F., G. R. McGregor, and C. Kidd, 2004: Diurnal cycle of rainfall over the Brazilian Amazon. *Climate Res.,* **26,** 139–149, doi:10.3354/cr026139.

Ashley, W. S., T. L. Mote, P. G. Dixon, S. L. Trotter, E. J. Powell, J. D. Durkee, and A. J. Grundstein, 2003: Distribution of mesoscale convective complex rainfall in the United States. *Mon. Wea. Rev.,* **131,** 3003–3017.

Awaka, J., T. Iguchi, H. Kumagai, and K. Okamoto, 1997: Rain type classification algorithm for TRMM Precipitation Radar. *Proc. 1997 Int. Geoscience and Remote Sensing Symp. (IGARSS '97)—Remote Sensing: A Scientific Vision for Sustainable Development,* Vol. 4, Singapore, IEEE, 1633–1635.

Carlson, T. N., S. G. Benjamin, G. S. Forbes, and Y. Li, 1983: Elevated mixed layers in the regional severe storm environment: Conceptual model and case studies. *Mon. Wea. Rev.,* **111,** 1453–1474.

Carvalho, L. M. V., C. Jones, and M. A. F. Silva Dias, 2002: Intraseasonal large-scale circulations and mesoscale convective activity in tropical South America during the TRMM-LBA campaign. *J. Geophys. Res.,* **107,** 8042, doi:10.1029/2001JD000745.

——, ——, and B. Liebmann, 2004: The South Atlantic convergence zone: Intensity, form, persistence, and relationships with intraseasonal to interannual activity and extreme rainfall. *J. Climate,* **17,** 88–108.

Cifelli, R., W. A. Petersen, L. D. Carey, S. A. Rutledge, and M. A. F. Silva Dias, 2002: Radar observations of the kinematic, microphysical, and precipitation characteristics of two MCSs in TRMM LBA. *J. Geophys. Res.,* **107,** 8077, doi:10.1029/2000JD000264.

Fritsch, J. M., R. J. Kane, and C. R. Chelius, 1986: The contribution of mesoscale convective weather systems to the warm-season precipitation in the United States. *J. Climate Appl. Meteor.,* **25,** 1333–1345.

Gan, M. A., and V. B. Rao, 1991: Surface cyclogenesis over South America. *Mon. Wea. Rev.,* **119,** 1293–1302.

——, V. E. Kousky, and C. F. Ropelewski, 2004: The South America monsoon circulation and its relationship to rainfall over west-central Brazil. *J. Climate,* **17,** 47–66.

Garreaud, R. D., 2000: Cold air incursions over subtropical South America: Mean structure and dynamics. *Mon. Wea. Rev.,* **128,** 2544–2559.

——, and J. M. Wallace, 1997: The diurnal march of convective cloudiness over the Americas. *Mon. Wea. Rev.,* **125,** 3157–3171.

——, and ——, 1998: Summertime incursions of midlatitude air into subtropical and tropical South America. *Mon. Wea. Rev.,* **126,** 2713–2733.

Garstang, M., H. L. Massie, J. Halverson, S. Greco, and J. Scala, 1994: Amazon coastal squall lines. Part I: Structure and kinematics. *Mon. Wea. Rev.,* **122,** 608–622.

Giovannettone, J. P., and A. P. Barros, 2009: Probing regional orographic controls of precipitation and cloudiness in the central Andes using satellite data. *J. Hydrometeor.,* **10,** 167–182.

Halverson, J. B., T. Rickenbach, B. Roy, H. Pierce, and E. Williams, 2002: Environmental characteristics of convective systems during TRMM-LBA. *Mon. Wea. Rev.,* **130,** 1493–1509.

Houze, R. A., Jr., 2004: Mesoscale convective systems. *Rev. Geophys.,* **42,** RG4003, doi:10.1029/2004RG000150.

——, D. C. Wilton, and B. F. Smull, 2007: Monsoon convection in the Himalayan region as seen by the TRMM Precipitation Radar. *Quart. J. Roy. Meteor. Soc.,* **133,** 1389–1411, doi:10.1002/qj.106.

Huffman, G. J., and Coauthors, 2007: The TRMM Multisatellite Precipitation Analysis (TMPA): Quasi-global, multiyear, combined-sensor precipitation estimates at fine scales. *J. Hydrometeor.,* **8,** 38–55.

Iguchi, T., R. Meneghini, J. Awaka, T. Kozu, and K. Okamoto, 2000: Rain profiling algorithm for TRMM Precipitation Radar data. *Adv. Space Res.,* **25,** 973–976, doi:10.1016/S0273-1177(99)00933-3.

Jones, C., and L. M. V. Carvalho, 2002: Active and break phases in the South American monsoon system. *J. Climate,* **15,** 905–914.

Kalnay, E., and Coauthors, 1996: The NCEP/NCAR 40-Year Reanalysis Project. *Bull. Amer. Meteor. Soc.,* **77,** 437–471.

Kikuchi, K., and B. Wang, 2008: Diurnal precipitation regimes in the global tropics. *J. Climate,* **21,** 2680–2696.

Kousky, V. E., and L. C. B. Molion, 1981: Uma contribuição à climatologia da dinâmica da troposfera sobre a Amazônia. *Rev. Bras. Hidrol. Recursos Hidricos,* **3,** 199–211.

Kozu, T., R. Meneghini, J. Awaka, and K. Okamoto, 2000: Rain-profiling algorithm for the TRMM Precipitation Radar. *J. Appl. Meteor.,* **39,** 2038–2052.

Kummerow, C., W. Barnes, T. Kozu, J. Shiue, and J. Simpson, 1998: The Tropical Rainfall Measuring Mission (TRMM) sensor package. *J. Atmos. Oceanic Technol.,* **15,** 809–817.

——, and Coauthors, 2000: The status of the Tropical Rainfall Measuring Mission (TRMM) after two years in orbit. *J. Appl. Meteor.,* **39,** 1965–1982.

Laurent, H., L. A. T. Machado, C. A. Morales, and L. Durieux, 2002: Characteristics of the Amazonian mesoscale convective systems observed from satellite and radar during the WETAMC/LBA experiment. *J. Geophys. Res.,* **107,** 8054, doi:10.1029/2001JD000337.

Lenters, J. D., and K. H. Cook, 1995: Simulation and diagnosis of the regional summertime precipitation climatology of South America. *J. Climate,* **8,** 2988–3005.

Liebmann, B., G. N. Kiladis, J. A. Marengo, T. Ambrizzi, and J. D. Glick, 1999: Submonthly convective variability over South America and the South Atlantic convergence zone. *J. Climate,* **12,** 1877–1891.

——, ——, C. S. Vera, A. C. Saulo, and L. M. V. Carvalho, 2004: Subseasonal variations of rainfall in South America in the vicinity of the low-level jet east of the Andes and comparison to those in the South Atlantic convergence zone. *J. Climate,* **17,** 3829–3842.

Liu, C., E. J. Zipser, D. J. Cecil, S. W. Nesbitt, and S. Sherwood, 2008: A cloud and precipitation feature database from nine years of TRMM observations. *J. Appl. Meteor. Climatol.,* **47,** 2712–2728.

Machado, L. A. T., and H. Laurent, 2004: The convective system area expansion over Amazonia and its relationships with convective system life duration and high-level wind divergence. *Mon. Wea. Rev.,* **132,** 714–725.

——, W. B. Rossow, R. L. Guedes, and A. W. Walker, 1998: Life cycle variations of mesoscale convective systems over the Americas. *Mon. Wea. Rev.,* **126,** 1630–1654.

——, H. Laurent, and A. A. Lima, 2002: Diurnal march of the convection observed during TRMM-WETAMC/LBA. *J. Geophys. Res.,* **107,** 8064, doi:10.1029/2001JD000338.

——, ——, N. Dessay, and I. Miranda, 2004: Seasonal and diurnal variability of convection over the Amazonia: A comparison of different vegetation types and large scale forcing. *Theor. Appl. Climatol.,* **78,** 61–77, doi:10.1007/s00704-004-0044-9.

Madden, R. A., and P. R. Julian, 1994: Observations of the 40–50-day tropical oscillation—A review. *Mon. Wea. Rev.,* **122,** 814–837.

Mapes, B. E., T. T. Warner, and M. Xu, 2003: Diurnal patterns of rainfall in northwestern South America. Part III: Diurnal gravity waves and nocturnal convection offshore. *Mon. Wea. Rev.,* **131,** 830–844.

Marengo, J. A., W. R. Soares, C. Saulo, and M. Nicolini, 2004: Climatology of the low-level jet east of the Andes as derived from the NCEP–NCAR reanalyses: Characteristics and temporal variability. *J. Climate,* **17,** 2261–2280.

Medina, S., R. A. Houze, A. Kumar, and D. Niyogi, 2010: Summer monsoon convection in the Himalayan region: Terrain and land cover effects. *Quart. J. Roy. Meteor. Soc.,* **136,** 593–616.

Meneghini, R., J. A. Jones, T. Iguchi, K. Okamoto, and J. Kwiatkowski, 2001: Statistical methods of estimating average rainfall over large space–time scales using data from the TRMM Precipitation Radar. *J. Appl. Meteor.,* **40,** 568–585.

Molion, L. C. B., 1987: Climatologia dinâmica da região Amazônica: Mecanismos de precipitação. *Rev. Bras. Meteor.,* **2,** 107–177.

Negri, A. J., E. N. Anagnostou, and R. F. Adler, 2000: A 10-yr climatology of Amazonian rainfall derived from passive microwave satellite observations. *J. Appl. Meteor.,* **39,** 42–56.

——, T. L. Bell, and L. Xu, 2002a: Sampling of the diurnal cycle of precipitation using TRMM. *J. Atmos. Oceanic Technol.,* **19,** 1333–1344.

——, L. Xu, and R. F. Adler, 2002b: A TRMM-calibrated infrared rainfall algorithm applied over Brazil. *J. Geophys. Res.,* **107,** 8048, doi:10.1029/2000JD000265.

Nicolini, M., and A. C. Saulo, 2006: Modeled Chaco low-level jets and related precipitation patterns during the 1997–1998 warm season. *Meteor. Atmos. Phys.,* **94,** 129–143, doi:10.1007/s00703-006-0186-7.

Nieto Ferreira, R., T. M. Rickenbach, D. L. Herdies, and L. M. V. Carvalho, 2003: Variability of South American convective cloud systems and tropospheric circulation during January–March 1998 and 1999. *Mon. Wea. Rev.,* **131,** 961–973.

Nogués-Paegle, J., and K. C. Mo, 1997: Alternating wet and dry conditions over South America during summer. *Mon. Wea. Rev.,* **125,** 279–291.

Pereira, L. G., and S. A. Rutledge, 2006: Diurnal cycle of shallow and deep convection for a tropical land and an ocean environment and its relationship to synoptic wind regimes. *Mon. Wea. Rev.,* **134,** 2688–2701.

Petersen, W. A., S. W. Nesbitt, R. J. Blakeslee, R. Cifelli, P. Hein, and S. A. Rutledge, 2002: TRMM observations of intraseasonal variability in convective regimes over the Amazon. *J. Climate,* **15,** 1278–1294.

Rickenbach, T. M., 2004: Nocturnal cloud systems and the diurnal variation of clouds and rainfall in southwestern Amazonia. *Mon. Wea. Rev.,* **132,** 1201–1219.

——, R. Nieto Ferreira, J. B. Halverson, D. L. Herdies, and M. A. F. Silva Dias, 2002: Modulation of convection in the southwestern Amazon basin by extratropical stationary fronts. *J. Geophys. Res.,* **107,** 8040, doi:10.1029/2000JD000263.

Romatschke, U., S. Medina, and R. A. Houze, 2010: Regional, seasonal, and diurnal variations of extreme convection in the South Asian region. *J. Climate,* **23,** 419–439.

Rosenfeld, D., W. L. Woodley, T. W. Krauss, and V. Makitov, 2006: Aircraft microphysical documentation from cloud base to anvils of hailstorm feeder clouds in Argentina. *J. Appl. Meteor. Climatol.,* **45,** 1261–1281.

Salio, P., M. Nicolini, and E. J. Zipser, 2007: Mesoscale convective systems over southeastern South America and their relationship with the South American low-level jet. *Mon. Wea. Rev.,* **135,** 1290–1309.

Saulo, A. C., M. Nicolini, and S. C. Chou, 2000: Model characterization of the South American low-level flow during the 1997–1998 spring–summer season. *Climate Dyn.,* **16,** 867–881, doi:10.1007/s003820000085.

Silva Dias, M. A. F., and Coauthors, 2002: Cloud and rain processes in a biosphere-atmosphere interaction context in the Amazon region. *J. Geophys. Res.,* **107,** 8072, doi:10.1029/2001JD000335.

Velasco, I., and J. M. Fritsch, 1987: Mesoscale convective complexes in the Americas. *J. Geophys. Res.,* **92,** 9591–9613.

Vera, C., and Coauthors, 2006: Toward a unified view of the American monsoon systems. *J. Climate,* **19,** 4977–5000.

Zipser, E. J., D. J. Cecil, C. Liu, S. W. Nesbitt, and D. P. Yorty, 2006: Where are the most intense thunderstorms on earth? *Bull. Amer. Meteor. Soc.,* **87,** 1057–1071.